Computer Modeling of Laser-Excited Molecular and Atomic-Molecular Systems

D. H. Campbell
ARO, Inc.

August 1981

Final Report for Period October 1, 1979 — September 1, 1980

**ARNOLD ENGINEERING DEVELOPMENT CENTER
ARNOLD AIR FORCE STATION, TENNESSEE
AIR FORCE SYSTEMS COMMAND
UNITED STATES AIR FORCE**

This report has been reviewed by the Office of Public Affairs (PA) and is releasable to the National Technical Information Service (NTIS). At NTIS, it will be available to the general public, including foreign nations.

APPROVAL STATEMENT

This report has been reviewed and approved.

KENNETH H. LENERS, Captain, USAF
Directorate of Technology
Deputy for Operations

Approved for publication:

FOR THE COMMANDER

MARION L. LASTER
Director of Technology
Deputy for Operations

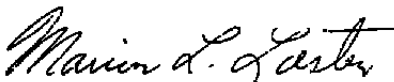| REPORT DOCUMENTATION PAGE		READ INSTRUCTIONS BEFORE COMPLETING FORM
1 REPORT NUMBER AEDC-TR-80-47	2 GOVT ACCESSION NO.	3 RECIPIENT'S CATALOG NUMBER
4 TITLE (and Subtitle) COMPUTER MODELING OF LASER-EXCITED MOLEC-ULAR AND ATOMIC-MOLECULAR SYSTEMS		5 TYPE OF REPORT & PERIOD COVERED Final Report - Oct. 1, 1979 - Sept. 1, 1980
		6. PERFORMING ORG REPORT NUMBER
7 AUTHOR(s) D. H. Campbell, ARO. Inc., a Sverdrup Corporation Company		8 CONTRACT OR GRANT NUMBER(s)
9 PERFORMING ORGANIZATION NAME AND ADDRESS Arnold Engineering Development Center/DOT Air Force Systems Command Arnold Air Force Station, TN 37389		10 PROGRAM ELEMENT, PROJECT TASK AREA & WORK UNIT NUMBERS Program Element 65807F
11 CONTROLLING OFFICE NAME AND ADDRESS Arnold Engineering Development Center/DOS Air Force Systems Command Arnold Air Force Station, TN 37389		12 REPORT DATE August 1981
		13 NUMBER OF PAGES 45
14 MONITORING AGENCY NAME & ADDRESS(if different from Controlling Office)		15 SECURITY CLASS. (of this report) UNCLASSIFIED
		15a DECLASSIFICATION DOWNGRADING SCHEDULE N/A

16 DISTRIBUTION STATEMENT (of this Report)

Approved for public release: distribution unlimited.

17 DISTRIBUTION STATEMENT (of the abstract entered in Block 20, if different from Report)

18 SUPPLEMENTARY NOTES

Available in Defense Technical Information Center (DTIC).

19 KEY WORDS (Continue on reverse side if necessary and identify by block number)

laser induced fluorescence
Raman spectroscopy
gas analysis
combustion

computerized simulation
electronic states
diatomic molecules
carbon monoxide

20 ABSTRACT (Continue on reverse side if necessary and identify by block number)

The potential application of the laser-induced fluorescence method for determining number densities and temperatures of gas species is investigated through computer modeling of the detailed relaxation of laser-excited molecular and atomic-molecular systems. The rate equation models for a sodium-diatomic molecular system and a single diatomic molecule system are explained and applied to the case of sodium-nitrogen and pure carbon monoxide.

DD FORM 1473 EDITION OF 1 NOV 65 IS OBSOLETE
1 JAN 73

PREFACE

The research reported herein was performed by the Arnold Engineering Development Center (AEDC), Air Force Systems Command (AFSC). Work and analysis for this research were done by personnel of ARO, Inc., AEDC Group (a Sverdrup Corporation Company), operating contractor for the AEDC, AFSC, Arnold Air Force Station, Tenneseee. The work covered the period from October 1, 1979 to September 1, 1980 and was done under Project Number P32M-01A. Capt. K. H. Leners was the Air Force project manager. The manuscript was submitted for publication on September 11, 1980.

Mr. D. H. Campbell is currently employed at the Air Force Rocket Propulsion Laboratory, Edwards Air Force Base, CA.

CONTENTS

ILLUSTRATIONS

Figure

4

1.0 INTRODUCTION

Among the requirements encountered in ground-based simulation test facilities is the need to determine the gaseous composition, temperatures, and flow velocity in both simulation flow fields and the exhaust plumes of various engines. A variety of techniques are being developed and applied to such problems, but the measurement of the properties of minor species has been most difficult. This capability is desired to provide both spatially and temporally resolved measurements of the number densities of various low concentration, or minor, species in combusting flow fields and engine exhaust plumes, with OH, H, and, in some cases, H_2 being exemplary species.

It is known that for very low concentrations (mole fractions on the order of 10^{-2} or less) of such species, local measurements using Raman scattering are impractical because of low signal levels. However, fluorescence techniques do possess the necessary requisites of molecular specificity, and spatial and temporal resolution. Also, since fluorescence excitation cross sections exceed Raman scattering cross sections by over eight orders of magnitude, the sensitivity of fluorescence is exceptionally good. Further, unlike charged-particle fluorescence excitation, the laser-induced fluorescence (LIF) technique is energy eigenstate specific, which simplifies considerably the resulting fluorescence spectra. These advantages of LIF are lessened considerably, however, by recognition of the existence of quenching processes of the excited, radiating species, for now the radiation intensity is no longer a linear function of the local density. Furthermore, the degree of nonlinearity is a function of the number density of each species in the sample.

However, it is known that for sufficiently intense laser beam sources interacting with simple two- and three-energy level systems, the laser-induced stimulated emission predominates over the loss of excited state species by collisional quenching. Consequently, for such saturation conditions, collisional quenching is unimportant, and the laser-induced fluorescence provides a direct measurement of the local species density. Unfortunatly, most molecular species of interest are not accurately described by simple two- and three-level systems but rather are multi-state systems. To evaluate the feasibility and advantages of the use of laser-induced fluorescence for such species, it is necessary to describe analytically the response of such systems to intense laser beam sources and to determine the effects and importance of collisional quenching processes. This report describes the results of a study of the time-dependent fluorescent signal of a commonly encountered plume gas species CO.

During this study it became clear that even if saturation conditions were not achieved, a second method of application of LIF was possible if the fluorescent species was a trace gas species in a binary mixture. For a situation in which collisional quenching of the

fluorescence of the trace species exists, the fluorescence signal is a direct function of the local density of the host gas, or major species, of the mixture; i.e., for a specified excitation source the fluorescence response of the trace species is dominated and determined by the density of the quenching species, and this dependence should yield a direct measure of the major species density. To investigate the possibility of measurement of the density of the major species using tracer gas impurity fluorescence, it was decided to focus attention on a problem area for which such a technique would be useful — namely, the study of the boundary-layer properties of a low density N_2 nozzle expansion to which Na is added in very low concentrations as the tracer gas. The feasibility of applying this technique to such a problem was investigated by developing a theoretical description of the time-resolved fluorescence of Na in a N_2 host gas environment, and the results of this work are described in this report.

2.0 REVIEW OF LASER-INDUCED FLUORESCENCE (LIF) MODELS

The basic method of measuring gas species parameters by the laser-induced fluorescence (LIF) method is to excite an atom or molecule from the ground electronic state to an excited electronic state by absorption of visible or ultraviolet laser radiation. The subsequent fluorescence produced by spontaneous emission back to the ground electronic state is then measured. The intensity of the fluorescence is proportional to the total number density of atoms (or molecules) in the upper excited state from which the radiation originates. The total number density in the original excited ground state is then related to the upper state number density by an appropriate excitation-emission model. Finally, the total species number density is determined from an appropriate original distribution function over all the possible energy states which may be populated at the time of laser excitation. For molecular species, the temperature can be obtained by measuring the relative fluorescence intensities resulting from excitation of two or more ground state rotational-vibrational levels. For either temperature or number density measurements, the important step in obtaining values of those parameters with LIF is the excitation-emission model used to relate the measured fluorescent intensities to the original state of the gas species being investigated. The next two sections present the two most popular models used in LIF analysis, the two-level and three-level models.

2.1 TWO-LEVEL MODEL

The simplest excitation-emission model is the two-level model shown in Fig. 1. In this model it is assumed that the only important energy exchange processes are those which transfer energy between the two laser-coupled states. The rate equation for the population of level 2 can be written:

$$\frac{dN_2}{dt} = N_1 B_{12} \rho_\nu - \left[Q_{21} \cdot A_{21} + B_{21} \rho_\nu\right] N_2 \tag{1}$$

The notation for this and subsequent equations is described in the Nomenclature.
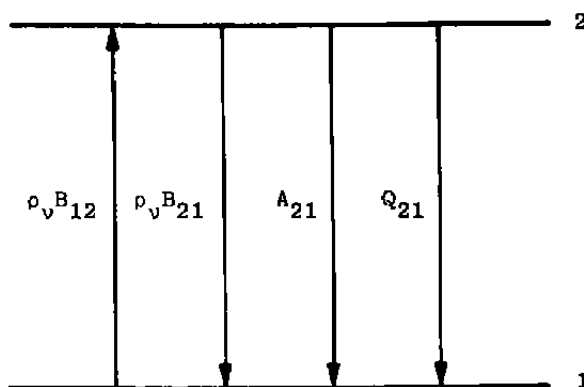
Figure 1. Two-level model schematic.

If it is assumed that at time $= 0$ all of the population is in level 1, then

$$N_T = N_1 + N_2 = N_1^o \tag{2}$$

For steady-state conditions the rate of change of population in level 2 is zero, and Eq. (1) can then be rearranged:

$$N_1^o = \frac{N_2\left[Q_{21} + A_{21} + (B_{12} + B_{21})\rho_\nu\right]}{B_{12}\rho_\nu} \tag{3}$$

which gives the ground state number density in terms of known (or measurable) constants and the number density in level 2, which is proportional to the fluorescent signal.

If the laser radiation density (ρ_ν) is large so that $(B_{12} + B_{21})\rho_\nu \gg Q_{21} + A_{21}$, saturation conditions exist, and Eq. (2) reduces to

$$N_1^o = \left(\frac{B_{12} + B_{21}}{B_{12}}\right) N_2 \tag{4}$$

which allows determination of the gas number density without the necessity of knowing the quenching rate Q_{21}.

Taking Eq. (2) and solving for N_2 and recognizing that the fluorescent signal (S) is related to the upper state number density by

$$S = C A_{21} N_2 \tag{5}$$

7

then

$$S = C A_{21} \ \frac{N_1^o \ B_{12}}{(Q_{21} + A_{21})/\rho_\nu + (B_{12} + B_{21})} \tag{6}$$

If a binomial expansion about $1/\rho_\nu$ is performed, the following expression is obtained:

$$S = C A_{21} \ \frac{B_{12}}{B_{12} - B_{21}} \ \left[N_1^o - \frac{N_1^o (Q_{21} - A_{21})}{\rho_\nu (B_{12} - B_{21})} + \ldots \right] \tag{7}$$

A plot of S versus $1/\rho_\nu$ will give N_1^o as a function of the intercept, and Q_{21} as a function of the slope (for known N_1^o). This "near" saturation technique provides another method for determining the number density without knowledge of Q_{21}. The two-level near-saturation technique has been used to measure number densities of C_2 (Ref. 1), MgO (Ref. 2), CH and CN (Ref. 3), and Na (Ref. 2) in flames. Additionally, OH number densities have been measured using the two-level model at low-pressure short pulse conditions to eliminate quenching effects (Ref. 4). Finally, Bechtal (Ref. 5) has used the two-level model with quenching effects included for measuring OH concentrations in a flame.

2.2 THREE-LEVEL MODEL

The three-level model, as shown schematically in Fig. 2, is particularly useful when two closely lying electronic states occur as the first excited levels above the ground state, as in sodium and potassium. For the case when level 2 is excited, the rate equation is

$$\frac{dN_2}{dt} = -\left[B_{21} \rho_\nu + A_{21} + Q_{21} + Q_{23} \right] N_2 + \left[B_{12} \rho_\nu + Q_{12} \right] N_1 + Q_{32} N_3 \tag{8}$$

Assuming that all of the population is in level 1 before laser excitation, then

$$N_T = N_1 + N_2 + N_3 = N_1^o \tag{9}$$

At steady-state, Eq. (6) can be rearranged:

$$N_1^o = \frac{\left[(B_{21} - B_{12}) \rho_\nu - A_{21} + Q_{21} + Q_{12} + Q_{23} \right] N_2 - \left[Q_{32} - Q_{12} - B_{12} \rho_\nu \right] N_3}{B_{12} \rho_\nu + Q_{12}} \tag{10}$$

If all quenching and collisional exchange rates are known, then N_1^o can be determined from the total fluorescent signal from levels 1 and 2. Under saturated conditions Eq. (10) reduces to

$$N_1^o = N_3 + \left(\frac{B_{12} + B_{21}}{B_{12}} \right) N_2 \tag{11}$$

which would allow calculation of N_1^o from LIF measurements without the necessity of knowing the various collisional quenching and exchange rates. The three-level saturated LIF technique has been used to measure Na number densities in a flame (Ref. 6).
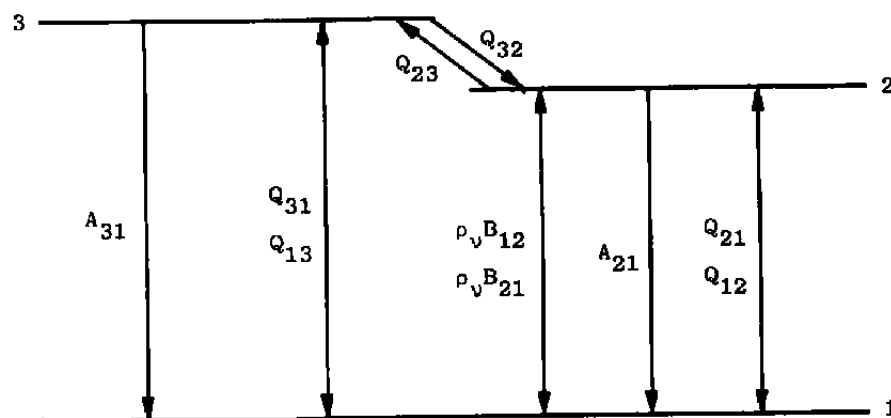
Figure 2. Three-level model schematic.

3.0 SODIUM-DIATOMIC MOLECULE SYSTEM RELAXATION

3.1 DETAILS OF QUENCHING MECHANISM

Experimental (Refs. 7 through 9) and theoretical (Ref. 10) analysis has shown that the collisional energy exchange collisions between sodium and diatomic molecules involve energy transfer between the electronic states of sodium and the vibrational state of the molecule. The quenching (Q_{21}, Q_{31}) and reverse quenching (Q_{12}, Q_{13}) rates in the rate equations for the sodium levels [Eq. (8)] are therefore dependent on the vibrational population distribution of the quenching molecule. Specifically,

$$Q_{21} = \sum_v N_v \sum_{w \geq v} k_{vw}$$

$$Q_{12} = \sum_w N_w \sum_{v \leq w} k'_{wv} \tag{12}$$

where k_{vw} is the rate constant (cm^3 sec^{-1}) for an upward vibrational transition causing a downward sodium transition (quenching), and k'_{wv} is the rate constant for a downward vibrational transition causing an upward sodium transition (reverse quenching). The upward and downward rate constants are related by the principle of detailed balancing:

9

$$k'_{wv} = k_{vw} \frac{g_2}{g_1} \exp\left[-(\Delta E_{21} - \Delta E_{vw})/kT\right] \tag{13}$$

where g_2 and g_1 and the statistical weight of sodium levels 2 and 1 (Fig. 2), ΔE_{21} is the sodium level energy difference, and ΔE_{vw} is the vibrational transition energy.

During an excitation-relaxation process in a sodium-diatomic mixture, the population in the vibrational levels of the quenching molecule may not maintain a Boltzmann distribution because of the relatively slow V-V exchange rates (Appendix A) and unequal sodium-molecule rate constants k_{vw} for different vibrational transitions. Consequently, the values of the total quenching and reverse quenching rates in Eqs. (8) and (10) may vary with time.

3.2 SODIUM-NITROGEN RELAXATION MODEL

To check the effects of the possible variation in quenching rates, a computer code was developed to calculate the time-dependent populations in all sodium electronic and molecular vibrational levels during laser excitation of one of the sodium 3S-3P transitions for nitrogen-sodium mixtures.

The rate equations for the ground electronic state ($3^2S_{1/2}$) and doublet first excited states ($3^2P_{1/2}$ and $3^2P_{3/2}$) of sodium are, for excitation of the $3^2P_{1/2}$ state (level 2):

$$\frac{dN_1}{dt} = -N_1\left[B_{12}\rho_\nu + \sum_w N_w \sum_{v\le w}(k'_{wv} + k''_{wv})\right] + N_2\left[B_{21}\rho_\nu - A_{21} + \sum_v N_v \sum_{w\ge v} k_{vw}\right]$$

$$+ N_3\left[A_{31} + \sum_v N_v \sum_{w\ge v} k_{vw}\right]$$

$$\frac{dN_2}{dt} = N_1\left[B_{12}\rho_\nu + \sum_w N_w \sum_{v\le w} k'_{wv}\right]$$

$$- N_2\left[B_{21}\rho_\nu - A_{21} + N_3 k_{23} + N_T k'_{23} + \sum_v N_v \sum_{w\ge v} k_{vw}\right] + N_3\left[N_2 k_{32} + N_T k'_{32}\right]$$

$$\frac{dN_3}{dt} = N_1 \sum_w N_w \sum_{v\le w} k''_{wv} - N_2\left[N_3 k_{23} + N_T k'_{23}\right]$$

$$- N_3\left[A_{31} + N_2 k_{32} + N_T k'_{32} + \sum_v N_v \sum_{w\ge v} k_{vw}\right] \tag{14}$$

where k_{32} and k_{23} are the P-level exchange rate constants for collisions with sodium atoms in the ground state ($3^2S_{1/2}$-level 1) and k'_{32} and k'_{23} are the P-level exchange rate constants for collisions with nitrogen molecules (total nitrogen number density = N_T). It is assumed that the quenching rate constants (k'_{wv} and k''_{wv} are equal for both P-levels, and the reverse quenching rate constants from detailed balancing are calculated [(Eq. (13)] so that for $v \le w$ $k'_{wv} \ne k''_{wv}$.

For a nitrogen vibrational level the rate equation broken into its component parts is

$$
\frac{dN_v}{dt} = -N_v \left[\sum_w N_w \left\{ R_{v,w;\,v+1,\,w-1} + R_{v,\,w,\,v-1,\,w+1} \right\} \right. \qquad \text{depleting VV}
$$

$$
\left. + N_T \sum_w R_{vw} \right] \qquad \text{depleting VT}
$$

$$
+ N_v \left[\sum_w N_w \left\{ R_{v+1,\,w;\,v,\,w-1} + R_{v-1,\,w;\,v,\,w+1} \right\} \right. \qquad \text{populating VV}
$$

$$
\left. + N_T \sum_w R_{wv} \right] \qquad \text{populating VT}
$$

$$
-N_v \left[N_1 \sum_{w \le v} (k'_{vw} + k''_{vw}) \right. \qquad \text{depleting reverse Q}
$$

$$
\left. + (N_2 + N_3) \sum_{w \ge v} k_{wv} \right] \qquad \text{depleting Q}
$$

$$
+ N_1 \sum_{w \ge v} N_w (k'_{wv} + k''_{wv}) \qquad \text{populating reverse Q}
$$

$$
+ (N_2 + N_3) \sum_{w \le v} N_w k_{wv} \qquad \text{populating Q} \qquad (15)
$$

The V-V and V-T rate constants are discussed in Appendix A.

If the complete system of sodium electronic level and nitrogen vibrational level rate equations and initial conditions of a Boltzmann distribution in the nitrogen vibrational

levels and all sodium population in the ground electronic state is used, the time-dependent populations are found by numerically solving the system of equations by the Gear linear multistep method (Ref. 11).

Table 1 lists the values of the energy exchange cross sections, along with some of the other atomic and molecular constants used in this analysis. The rate constants for use in the rate equations are calculated by multiplying the cross section by the relative speed of the colliding species, which is dependent on the gas temperature. The quenching rate constants are based on the change in vibrational level (Δv) during the quenching collision. A Gaussian-like distribution of the quenching probability is used, as suggested by the experimental scattering experiments of Ref. 12. Figure 3 shows the probability distribution used in the present work. Notice that the peak is placed at $v = 3$ and $v = 4$, not at the resonance condition ($\sim v = 8$). It is assumed that there is no dependence on the initial (or final) vibrational level. The actual quenching rate constants are calculated by taking the relative probabilities and, using a Boltzmann distribution at the gas temperature, summing the products of number density and quenching probability for each vibrational level and then normalizing so that

$$\sum_v N_v \sum_{w \geq v} k_{vw} = Q_{1j} \tag{16}$$

Table 1. Constants for Sodium-Nitrogen Model

Parameter	Value	Source
$A_{21} = A_{31}$	6.13×10^7 sec^{-1}	Ref. 17
q_{32}	283 Å^2	Ref. 18
q_{23}	552 Å^2	Detailed Balance
$q_{23}^{'*}$	144 Å^2	Ref. 14
$q_{32}^{'*}$	73.8 Å^2	Detailed Balance
$\lambda(3^2P_{1/2} - 3^2S_{1/2})$	5895.9 Å^2	Ref. 19
$\lambda(3^2P_{3/2} - 3^2S_{1/2})$	5889.9 Å	Ref. 19

*at 400°K

12
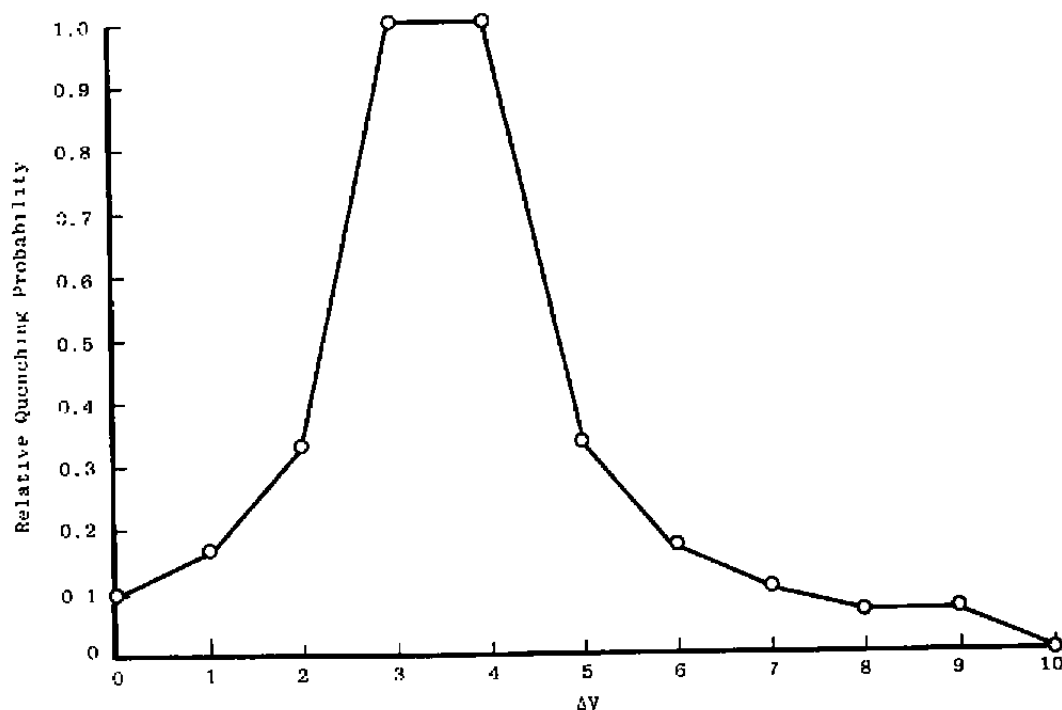
Figure 3. Sodium-nitrogen collisional quenching
probability distribution.

where Q_T is the total quenching rate (sec^{-1}). This rate is calculated, in turn, from a chosen total quenching cross section and the relative speed of the colliding species. The quenching rate constants for the sodium $3^2P_{3/2}$ and $3^2P_{1/2}$ levels are assumed to be equivalent. The reverse quenching rate constants are calculated from the quenching rate constants by detailed balancing Eq. (13). The reverse quenching-rate constants for the two sodium P levels will be similar but somewhat different in value because of the 17.3-cm^{-1} energy difference between the two P levels, and to the different statistical weights of the levels. The sodium-nitrogen total quenching cross sections ($q_{3l} = q_{2l}$) are taken from the review article by Lijnse and Elsenaar (Ref. 8), which shows an inverse temperature dependence of the total quenching cross section below about 1,000°K.

Figure 4 presents the rate constants for quenching and reverse quenching collisions between the sodium 3P levels and nitrogen for vibrational transitions originating (for quenching collisions) in the 0th vibrational level, at a temperature of 2,000°K. From the figure it is apparent that reverse quenching rates are small compared to quenching rates for the lower v levels but that at the higher v levels reverse quenching collision rates are comparable to quenching rates. As shall be seen in the next section, this relationship between the quenching and reverse quenching rates for different vibrational levels has a strong influence on the time history of the laser-excited sodium-nitrogen system.

13
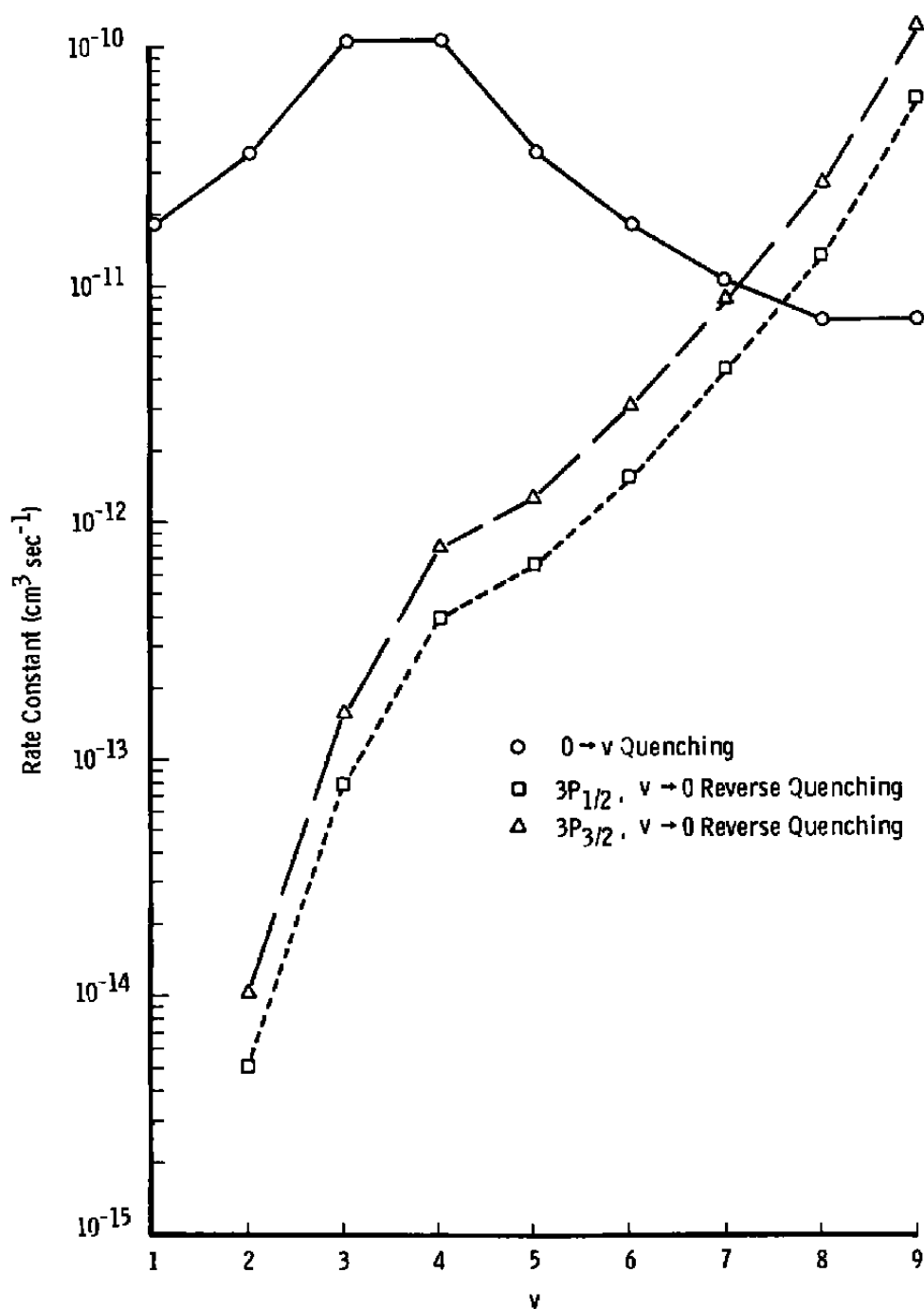
Figure 4. Quenching and reverse quenching rate constants
at T = 2,000°K.

The 3P level mixing exchange cross sections for collisions with molecules (q'_{23}, q'_{32}) are temperature adjusted using an exponential fit to the velocity-dependent cross section data of Ref. 13 along with the cross section at 400°K from Ref. 14. Figure 5 shows the cross sections and rate constants resulting from this procedure. Also shown in the figure is the rate constants which would result if a constant 3P mixing cross section were used. The application of a temperature correction on the 3P mixing cross section reduces the temperature dependence of the rate constant so that the rate constants at different temperature are more nearly equal. The 3P level mixing exchange cross sections for collisions with 3S sodium atoms (q_{23}, q_{32}) are not temperature-corrected because of a lack of information on the velocity dependence of these cross sections. However, the contribution of the 3S level collisional 3P mixing exchange rates on the relaxation in a sodium-nitrogen mixture is small because of the much lower sodium number densities compared to the nitrogen concentration for the conditions of interest.
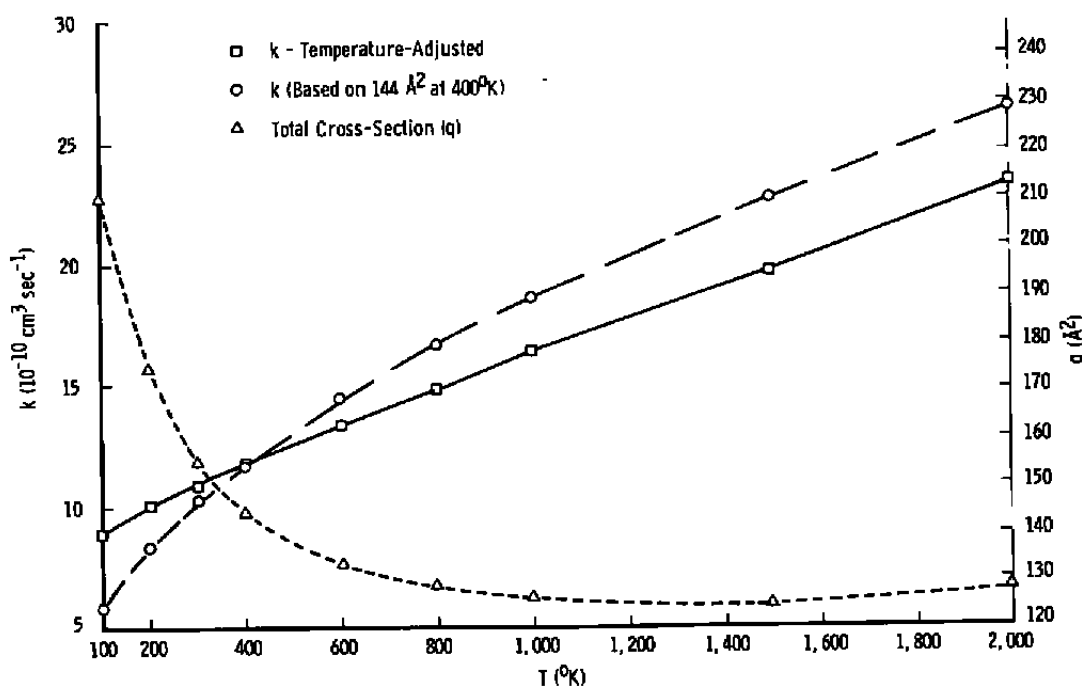
Figure 5. Sodium 3P level mixing exchange rate constants and total cross sections.

3.3 RESULTS OF SODIUM-NITROGEN MODELING

For relatively high number densities of nitrogen and sodium (2×10^{19} cm^{-3} and 1.0×10^{13}-cm^{-3}, respectively) and a temperature of 1,000°K, the time history of the

populations in the three sodium levels and in the nitrogen vibrational levels is shown in Figs. 6 and 7 for a constant laser radiation density (step function on at $t = 0$) of 1.0×10^{-10} ergs cm^{-3} Hz^{-1} exciting the $3P_{1/2}$ level. At this laser excitation energy, which is well below the saturation energy, the sodium level populations reach an equilibrium value after about 0.1 nsec, and maintain this constant level until approximately 0.1 msec, when a transition to a new steady-state level occurs. The vibrational population distribution continually changes as more and more molecules are put into higher vibrational levels, because of quenching collisions with sodium. The relatively slow V-V rates prevent the vibrational state from maintaining an equilibrium distribution, and eventually there is sufficient change from the original Boltzmann distribution to alter the total quenching cross section and to permit significant contributions from reverse quenching processes. For lower temperatures and/or higher laser intensities the results at these high number densities are qualitatively the same. For higher temperatures this is not the case, as illustrated in Figs. 8 and 9 for identical conditions to those in Figs. 6 and 7 except for a temperature of 2,000°K. At this temperature there is no transfer to a second steady-state condition. Despite the fact that there is a significant change in the vibrational population distribution, this change is not large enough to cause the transfer to a second steady-state condition. The vibrational population distribution attains a steady state after approximately 1 msec, so that there is no possibility of a change at times longer than those for which the calculation was performed.
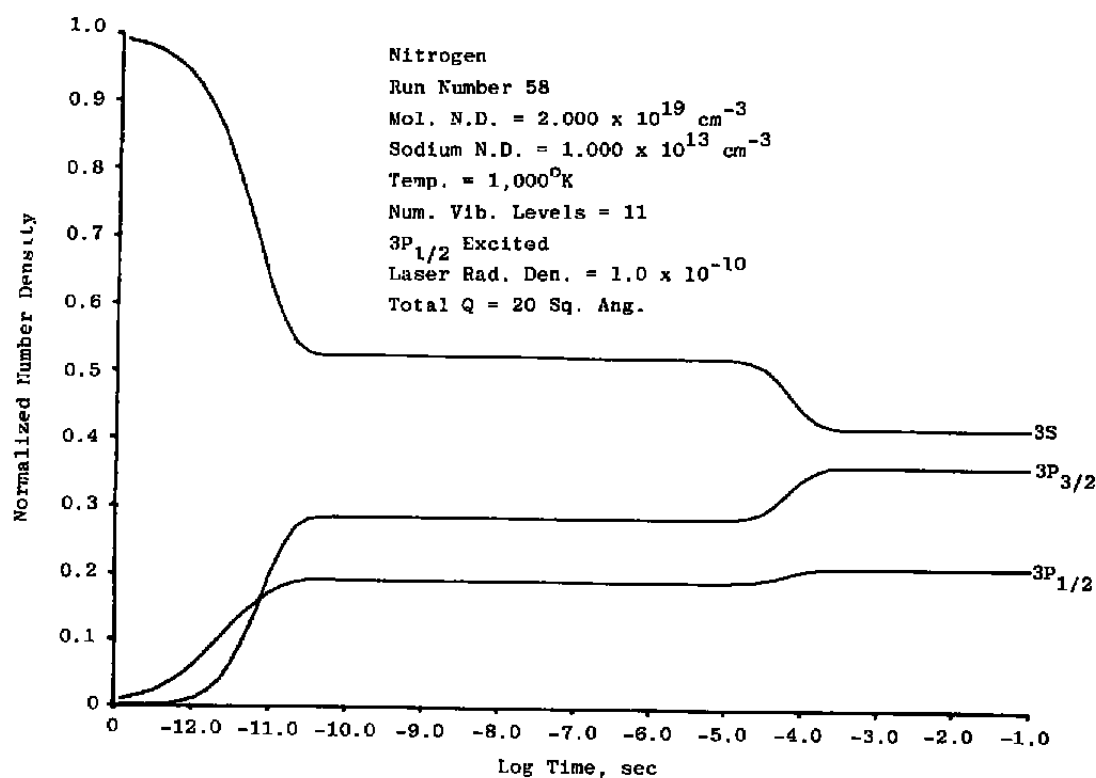
Figure 6. Time history of population in sodium levels for high density, T = 1,000°K.
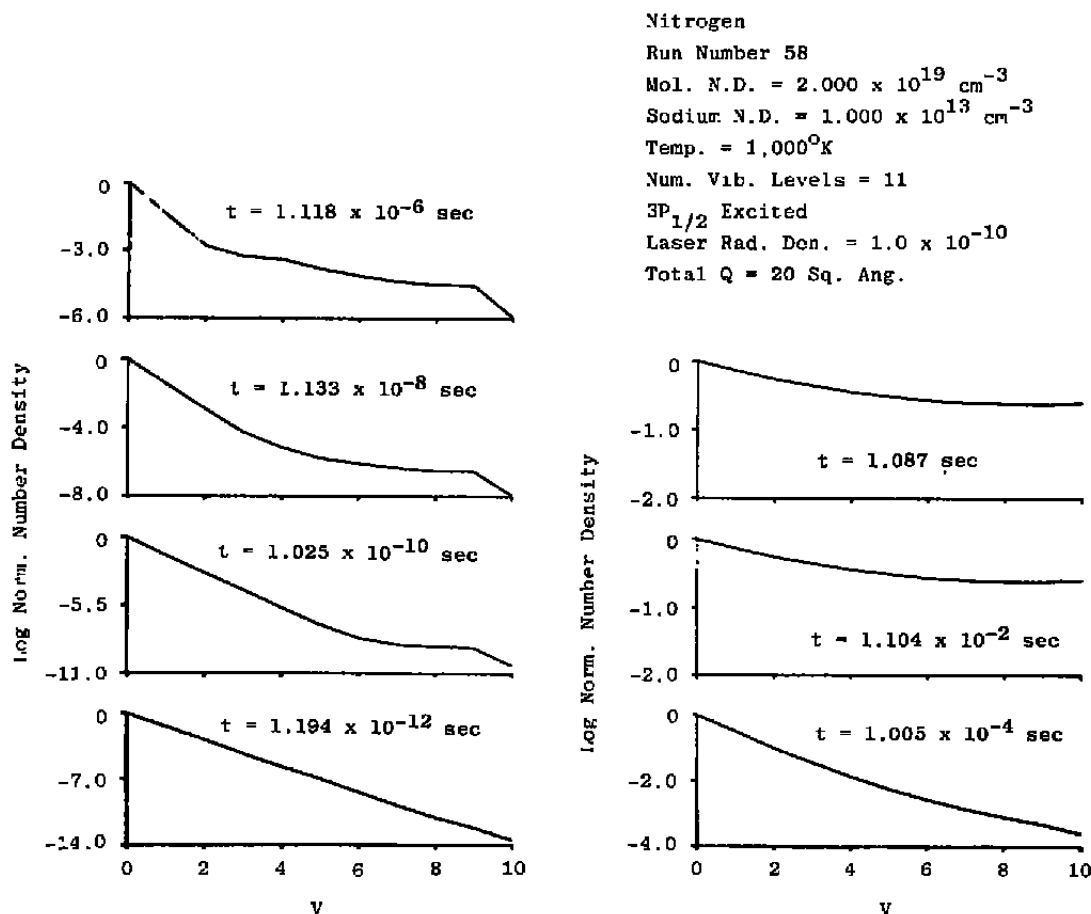
Figure 7. Time history of population in nitrogen vibrational levels
for high density, T = 1,000°K.

At lower number densities a still different picture emerges. Figure 10 shows the time history results for nitrogen and sodium number densities of 2.0×10^{17} and 1×10^{10} cm^{-3}, a temperature of 2,000°K and laser radiation density of 1.0×10^{-10} ergs cm^{-3} Hz^{-1}. The steady-state condition is not attained until after about 7 nsec with the $3P_{1/2}$ level showing a pronounced peak at about 0.2 nsec. This behavior occurs because of the dependence of the 3P level mixing exchange rates on the nitrogen number density. For these lower number densities the $3P_{3/2}$ populating collisions occur at a reduced rate so that the $3P_{3/2}$ level population process will lag the laser-excited $3P_{1/2}$ level population. At these conditions the $3P_{1/2}$ level attains a number density higher than its steady-state value before collisions with nitrogen, causing a transfer to the $3P_{3/2}$ level to become effective. After about 0.2 nsec this transfer process begins to depopulate the $3P_{1/2}$ level until the steady-state condition is obtained. At lower temperatures (Fig. 11) the same picture emerges with the exception that at very long times (~ 0.1 sec) a transition to a second steady-state condition occurs, because
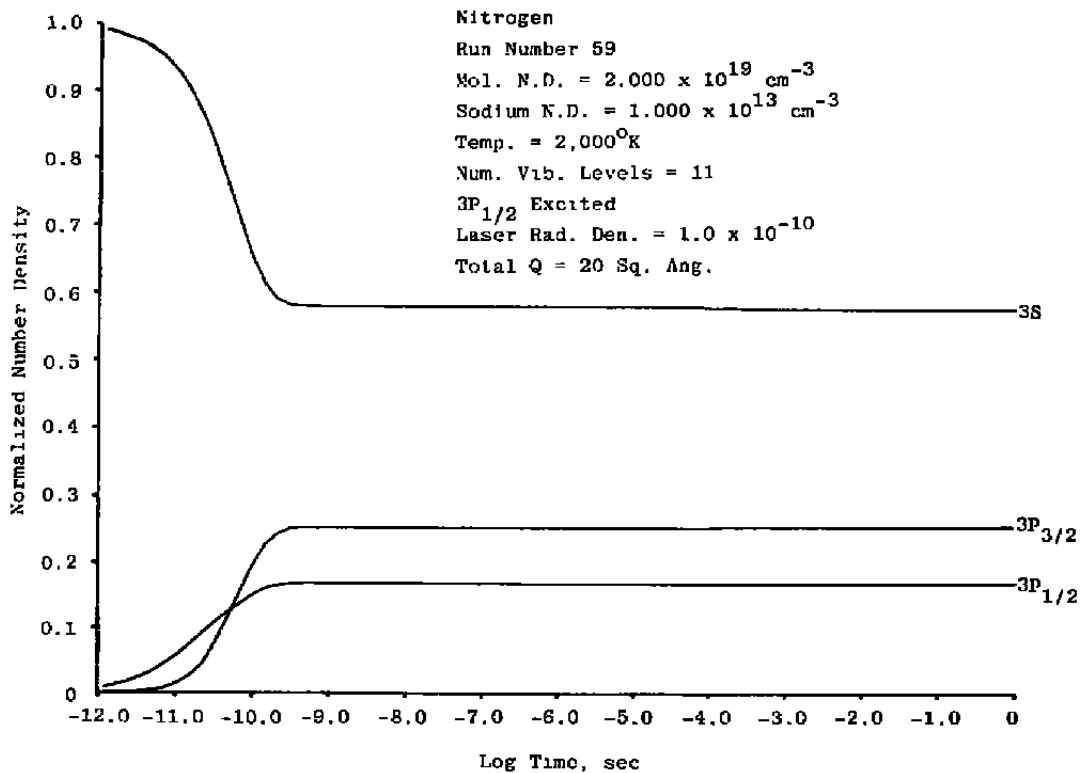
**Figure 8. Time history of population in sodium levels for
high density, T = 2,000°K.**

of the redistribution of population in the vibrational levels of nitrogen (Fig. 12). It takes a longer time at these conditions to attain sufficient population in the higher vibrational levels to cause the transfer to a second steady state than for the higher number density conditions. It should also be noted that at the same laser radiation density the system is closer to saturation (N_1 = N_2) at the lower nitrogen densities because of a reduction in the total quenching rate.

In summary, this analysis has shown that there can, in fact, be a significant effect on the relaxation of a sodium-nitrogen laser-excited system attributable to redistribution of vibrational population by quenching collisions. However, this effect occurs at sufficiently long times so that, for short laser pulse measurements (≤ 1 μsec) the steady-state relations [Eq. (10)] for a three-level system are applicable. On the other hand, extremely short pulses may not be long enough for steady state to be obtained under some conditions because of the finite 3P level exchange collision rate.

Nitrogen
Run Number 59
Mol. N.D. = 2.000 x 10^{19} cm^{-3}
Sodium N.D. = 1.000 x 10^{13} cm^{-3}
Temp. = 2,000°K
Num. Vib. Levels = 11
$3P_{1/2}$ Excited
Laser Rad. Den. = 1.0 x 10^{-10}
Total Q = 20 Sq. Ang.

t = 1.070 x 10^{-6} sec

t = 1.243 x 10^{-8} sec

t = 1.018 x 10^{-10} sec

t = 1.186 x 10^{-12} sec

t = 1.054 sec

t = 2.361 x 10^{-2} sec

t = 1.041 x 10^{-4} sec

Log Norm. Number Density

Log Norm. Number Density

V

V

Figure 9.   Time history of population in nitrogen vibrational levels
for high density, T = 2,000°K.

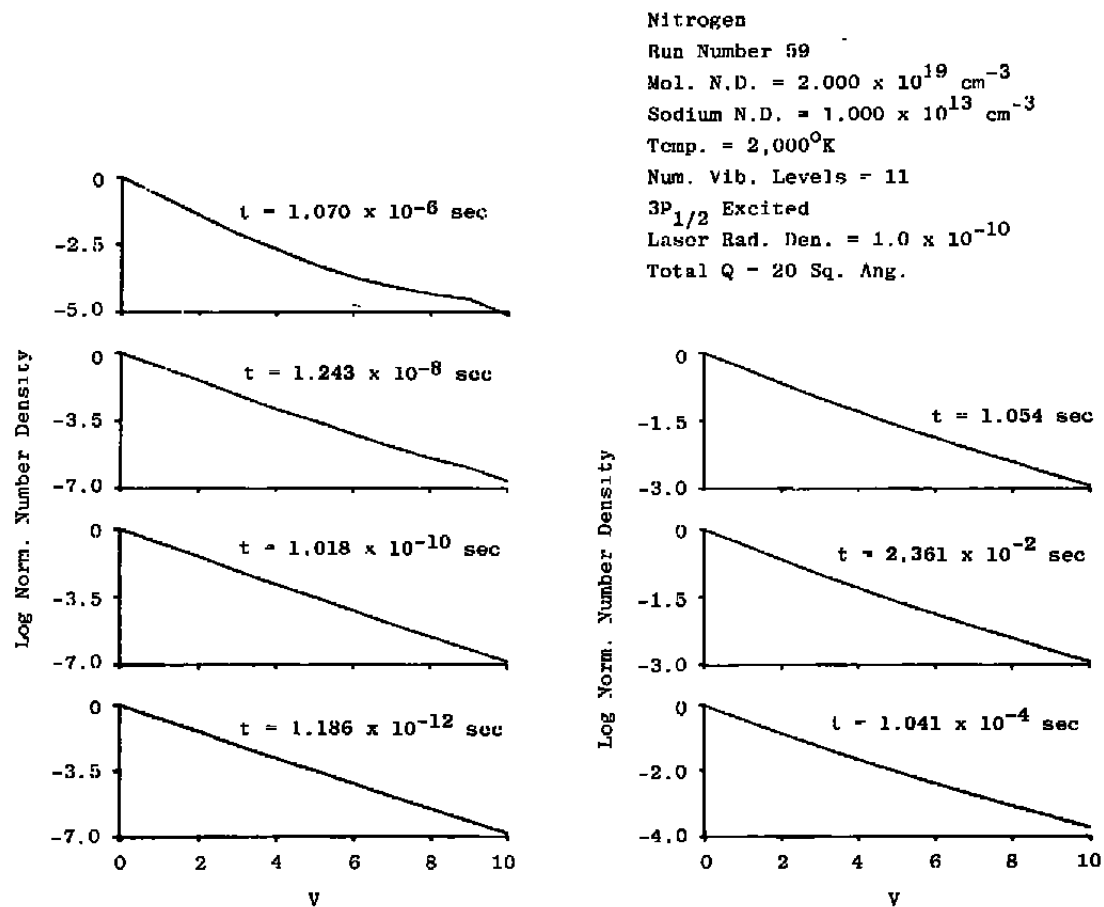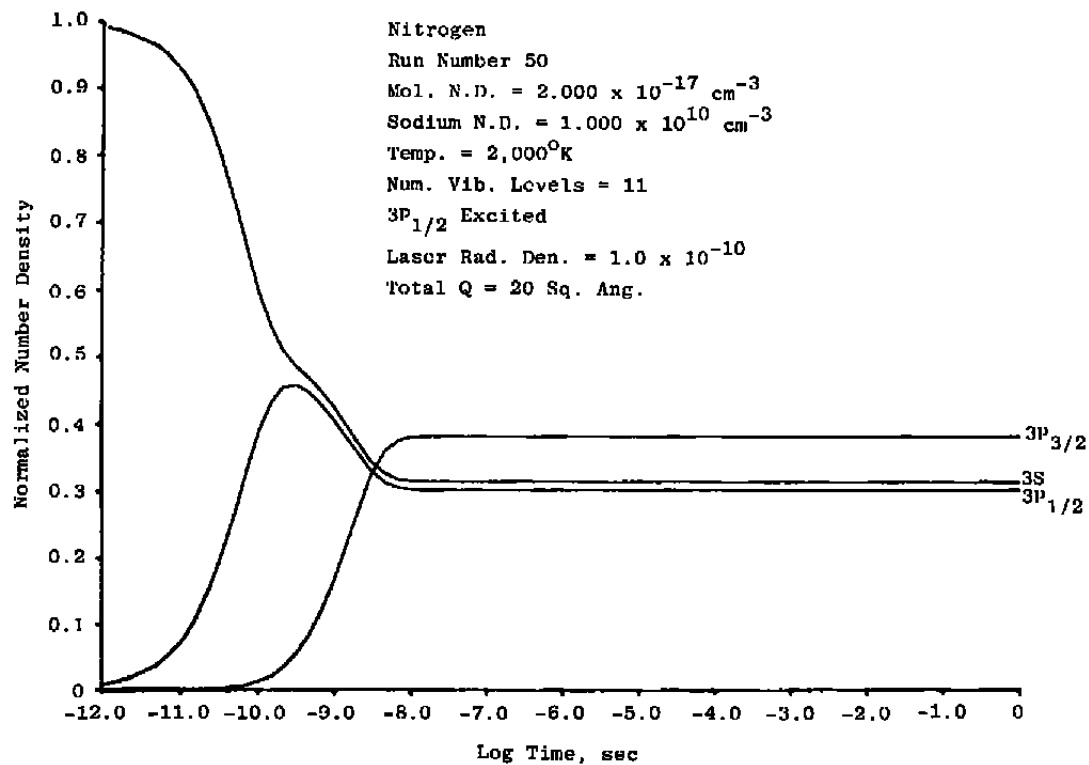Figure 10. Time history of population in sodium levels for low density, T = 2,000°K.
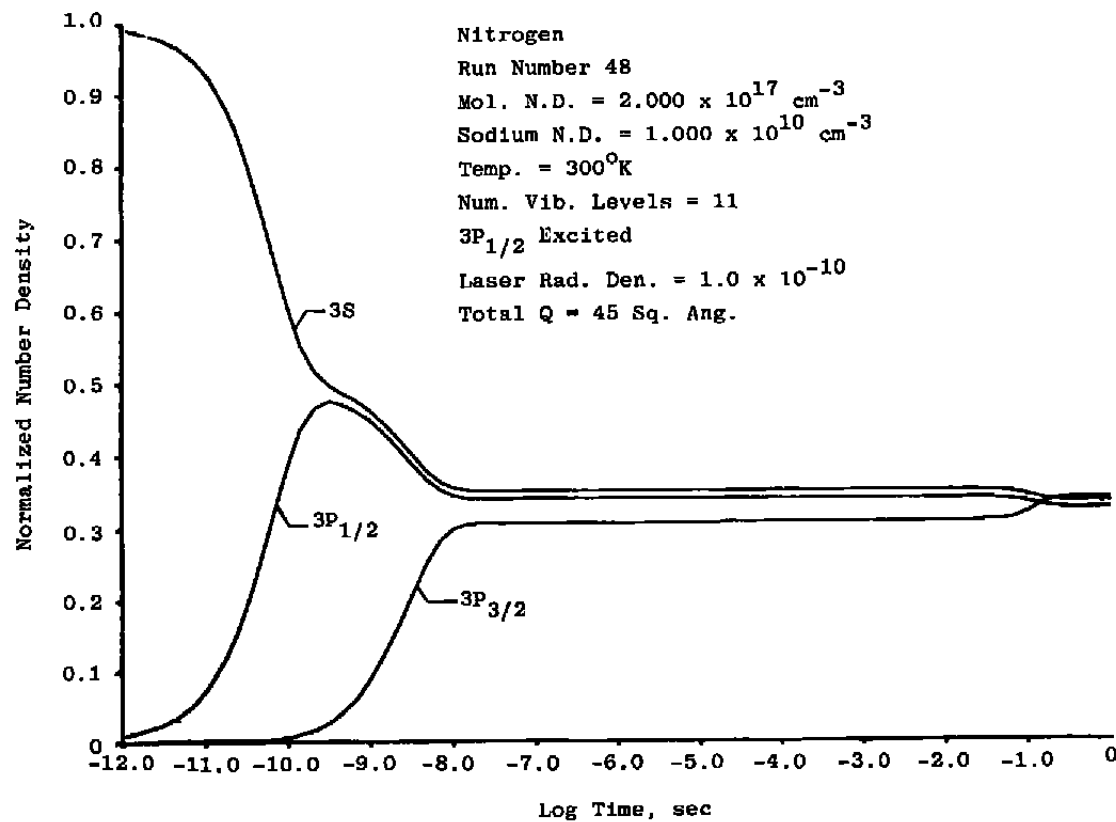
Figure 11. Time history of population in sodium levels for low density, T = 300°K.
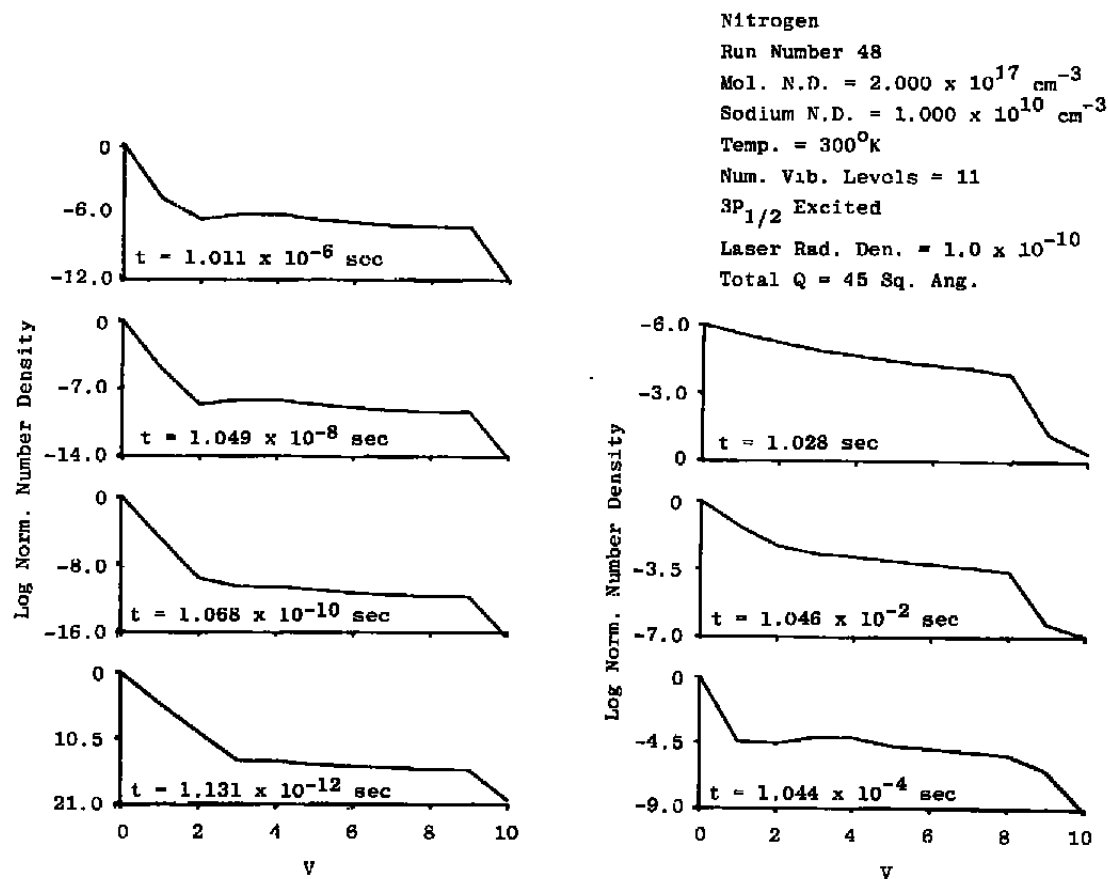
Figure 12. Time history of population in nitrogen vibrational levels
for low density, T = 300°K.

4.0 SINGLE DIATOMIC SPECIES RELAXATION

4.1 BREAKDOWN OF TWO-LEVEL MODEL ASSUMPTIONS

Real molecules contain complex rotational and vibrational structure which may cause significant breakdown of the assumptions in the two-level LIF model. Collisional energy exchange collisions during the laser excitation pulse will transfer energy between the laser-coupled vibrational-rotational states and the other vibrational-rotational states of the upper and lower electronic states at a finite rate. Additionally, spontaneous emission from the laser-populated upper level will occur not only to the laser-excited lower level, but also to other vibrational levels of the ground electronic state. Quenching collisions will also produce transitions to lower electronic vibrational-rotational states other than the laser-excited one. The possible effects of these processes will be:

1. Time-dependent populations and fluorescent intensities

2. Non-Boltzmann vibrational and rotational population distributions

3. Time dependent total number density in laser-coupled states [breakdown of Eq. (2)].

Lucht and Laurendeau (Ref. 15) have shown that when the ratio of the rotational relaxation rates of the upper and lower electronic states to the quenching rate are 100 or less, the steady-state rotational state population distributions are significantly non-Boltzmann. To investigate the steady-state vibrational population distribution and the time history of the rotational and vibrational distributions, a computer code has been constructed which follows the detailed relaxation of a diatomic molecule during laser excitation. The next section discusses the model used in the computer code.

4.2 SINGLE DIATOMIC SPECIES RELAXATION MODEL

For the case of a single diatomic species in which one particular vibrational-rotational (V-R) level in the ground electronic state of the molecule is pumped by laser radiation to one particular vibrational-rotational level in the first excited electronic state of the molecule, the following processes need to be considered:

1. Laser excitation and stimulated emission

2. Fluorescence from all upper electronic V-R states

3. Collisional exchange between rotation and translation (R-T)

4. Collisional exchange between the vibrational modes of collision partners (V-V)

5. Collisional exchange between vibration and translation (V-T)

6. Collisional quenching, i.e., nonradiative transitions from upper to lower electronic state

7. Radiative transitions between V-R levels of the same electronic state (heteronuclear molecules only)

8. Self-absorption of fluorescence

It is assumed that the gas is optically thin so that process 8 can be neglected. Additionally, the radiative lifetime for transitions between V-R levels of the same electronic state is typically much greater than the time scales for processes 1 through 6, so process 7 will also be neglected. Including processes 1 through 6, the rate equation for the lower electronic level, laser-excited V-R state is then (with its component parts specified):

$$\frac{dN_1(v'',J'')}{dt} = -N_1(v'',J'') \left[B_{12}\,\delta_\nu \right. \qquad \text{stimulated emission}$$

$$+ \sum_v N_1(v) \left\{ R_{v'',v;\,v''-1,\,v-1} + R_{v'',v;\,v''-1,\,v+1} \right\} \qquad \text{depleting VV}$$

$$\left. -N_T \left\{ \sum_v R_{v'',v} + \sum_J R_{J''J} \right\} \right] \qquad \text{depleting VT \& RT}$$

$$+ N_2(v',J') B_{21}\,\delta_\nu \qquad \text{laser absorption}$$

$$+ \sum_v \sum_J N_2(v,J) \left\{ A(v,J;\,v'',J'') - Q(v,J;\,v'',J'') \right\} \qquad \begin{array}{l}\text{radiation and}\\\text{quenching from}\\\text{upper electronic}\\\text{level}\end{array}$$

$$+ N_1(v'',J'') \left[\sum_v N_1(v) \left\{ R_{v''-1,v;\,v'',v-1} \right. \right.$$

$$\left. \left. + R_{v''-1,v;\,v'',v+1} \right\} \right. \qquad \text{populating VV}$$

$$+ N_T \left\{ \sum_v R_{vv''} + \sum_J R_{JJ''} \right\} \right]$$

$$(17)$$

Where v'' and J'' denote the laser-excited lower electronic state vibrational and rotational level, v' and J' denote the laser-excited upper electronic state vibrational and rotational level, N_1 and N_2 are the lower and upper electronic state number densities respectively, N_T is the total gas number density, B_{12} and B_{21} are the absorption and simulated emission coefficients, ϱ_ν is the laser radiation energy density, A the radiation rate (Einstein coefficient), Q the quenching rate, and the R's are the various collisional exchange rate constants (cm^{-3}/sec) which are identified by their subscripts. R_{vw} is the V-T rate constant for transfer from vibrational state v to vibrational state w', R_{IJ}; is the R-T rate constant for for transfer from rotational state J to state J', and $R_{v+1,w'; v, w+1}$ is the rate constant for V-V exchange for molecules in vibrational states $v + 1$ and w' colliding and exchanging vibrational energy to end up in states v and $w + 1$. For V-T and V-V processes, $|\Delta v| = 1$ transitions only are considered, but for R-T processes all ΔJ's are included in the analysis. The sum over J for the A and Q terms is limited to allowed dipple transitions only, i.e., P, Q, and R branch transitions in the case of CO. The quenching rates are based on the value of the Einstein A coefficients for the various vibrational-rotational transitions.

The rate equation for the laser-excited upper electronic V-R state is

$$\frac{dN_2 (v', J')}{dt} = -N_2 (v', J') \left[B_{21} P_\nu + \sum_v \sum_J \left(A (v', J'; v, J) + Q (v', J', v, J) \right) \right.$$

$$- \sum_v N_2 (v) (R_{v', v, v'+1, v-1} - R_{v', v; v'-1, v+1})$$

$$+ N_T \left(\sum_v R_{v'v} + \sum_J R_{J'J} \right) \left] + N_1 (v'', J'') B_{12} P_\nu \right.$$

$$+ N_2 (v', J') \left[\sum_v N_2 (v) (R_{v'+1, v; v', v-1} - R_{v'-1, v, v', v+1}) \right.$$

$$+ N_T \left(\sum_v R_{vv'} + \sum_J R_{JJ'} \right) \right]$$

$$(18)$$

The rate equations for the other V-R levels in the upper and lower electronic states are the same as those for the laser-coupled states without the absorption and stimulated emission terms.

25

4.3 CARBON MONOXIDE MODELING RESULTS

The total number of vibrational-rotational levels used in the relaxation model was restricted by computer time and core usage limitations; it was not possible to use a large number of rotational and vibrational levels simultaneously. The analysis was therefore divided into two parts. The first part used 31 rotational levels and 3 vibrational levels to investigate the rotational relaxation, and the second part neglected rotational relaxation and used 10 vibrational levels in each electronic state. For both test cases a step function laser pulse was applied at time t = 0 and a constant laser radiation density was maintained for the duration of the run time. Excitation is from a rotational level in the 0th vibrational level of the $X'\Sigma^+$ ground electronic state of CO up to one particular vibrational-rotational state in the $A'\Pi$ first excited electronic state. The absolute transition probabilities (Einstein A values) of Ref. 16 are used for the various vibrational transitions from the upper to the lower electronic state.

The time history of the rotational population distributions in the upper and lower laser-coupled vibrational levels is shown in Figs. 13 and 14 for atmospheric pressure conditions at 300°K and a laser radiation density of 1.0×10^{-8} ergs cm^{-3} Hz^{-1}, which is well under the saturation radiation density. The results agree qualitatively with those in Ref. 17. The distributions are highly non-Boltzmann with an overpopulation in the upper electronic state laser-pumped rotational level and an underpopulation in the lower electronic state laser-pumped rotational level.
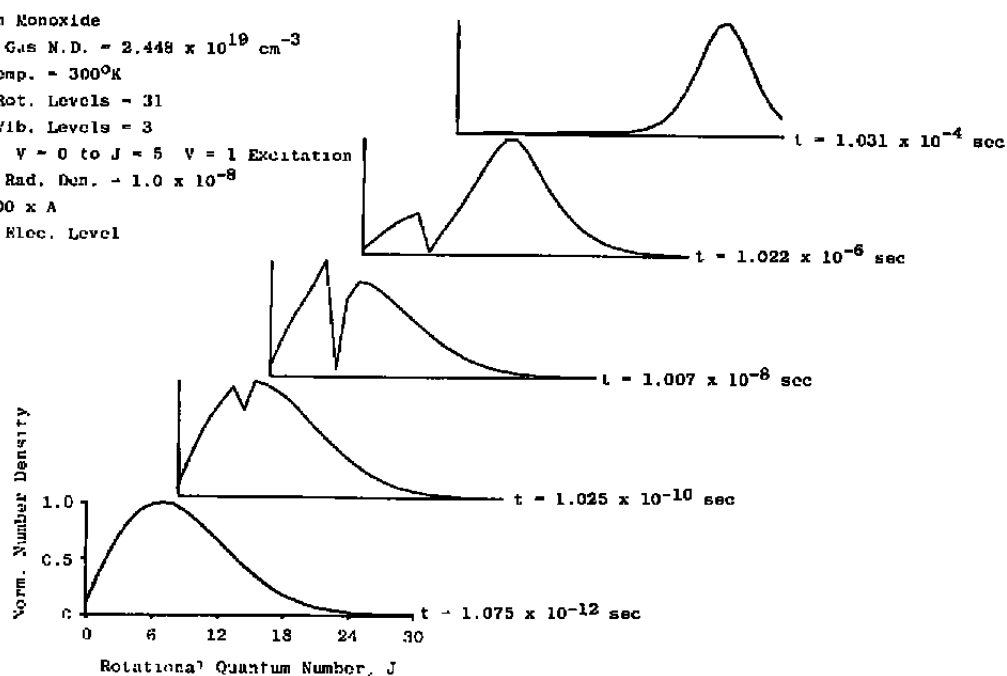
Figure 13. Time history of rotational population distribution in lower electronic state laser-coupled vibrational level.
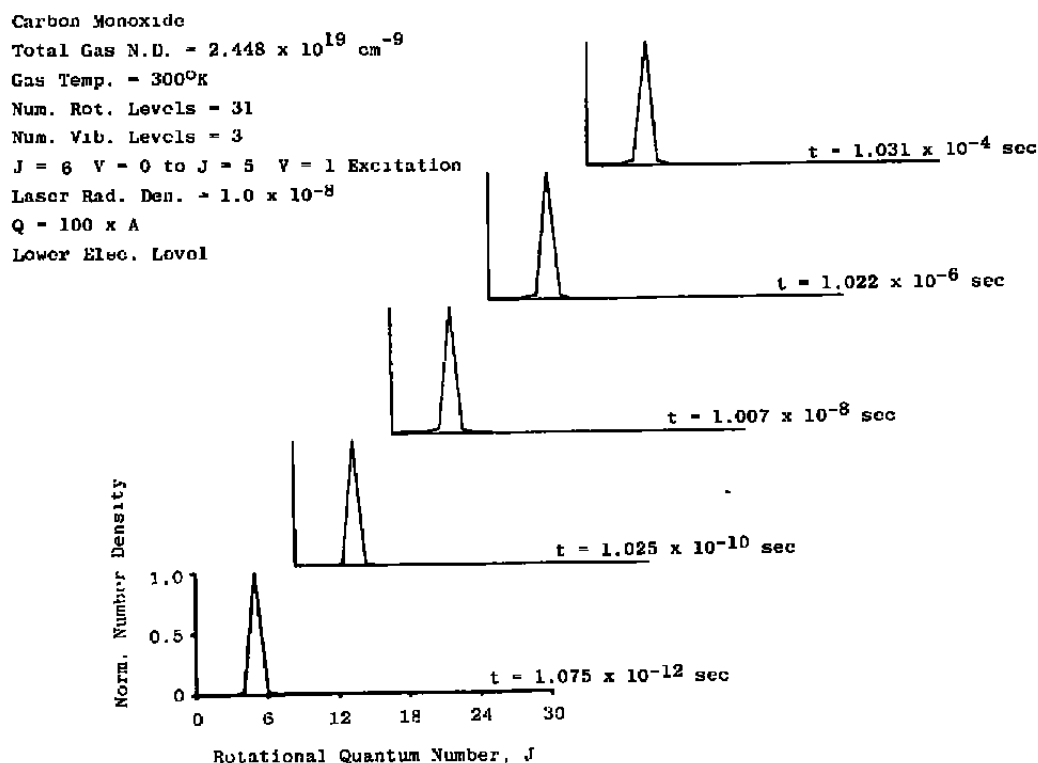
Figure 14. Time history of rotational population distribution in upper electronic state laser-coupled vibrational level.

For pure vibrational relaxation, Fig. 15 shows the time history of the number density of the upper electronic state laser-excited vibrational level for room temperature, atmospheric pressure conditions with three values of the quenching rate (Q). For all cases the population does not come to steady state until very long times (~0.1 sec). The initial drop in number density (around 0.1 nsec for $Q = 100$ x A) depends strongly on the quenching rate and is attributable to the depletion of population from the upper laser-excited state by quenching and radiative relaxation to the various ground electronic state vibrational levels where the finite V-V rates prevent fast enough collisional exchange to refill the depleted laser-excited vibrational level. Figures 16 and 17 show the time history of the vibrational population distributions in the upper and lower electronic states for $Q = 100$ x A. Highly non-Boltzmann distributions exist at all times during the relaxation. V-V collisional exchange tends to smooth out the vibrational population distribution in the ground electronic state, with the most pronounced effects occurring after about 1 msec. At a temperature of 2,000°K, (Fig. 18) the time history is qualitatively similar to that at 300°K except for a higher absolute steady-state number density at an earlier time. This effect is attributable to the much higher V-V and V-T rates at the higher temperature.
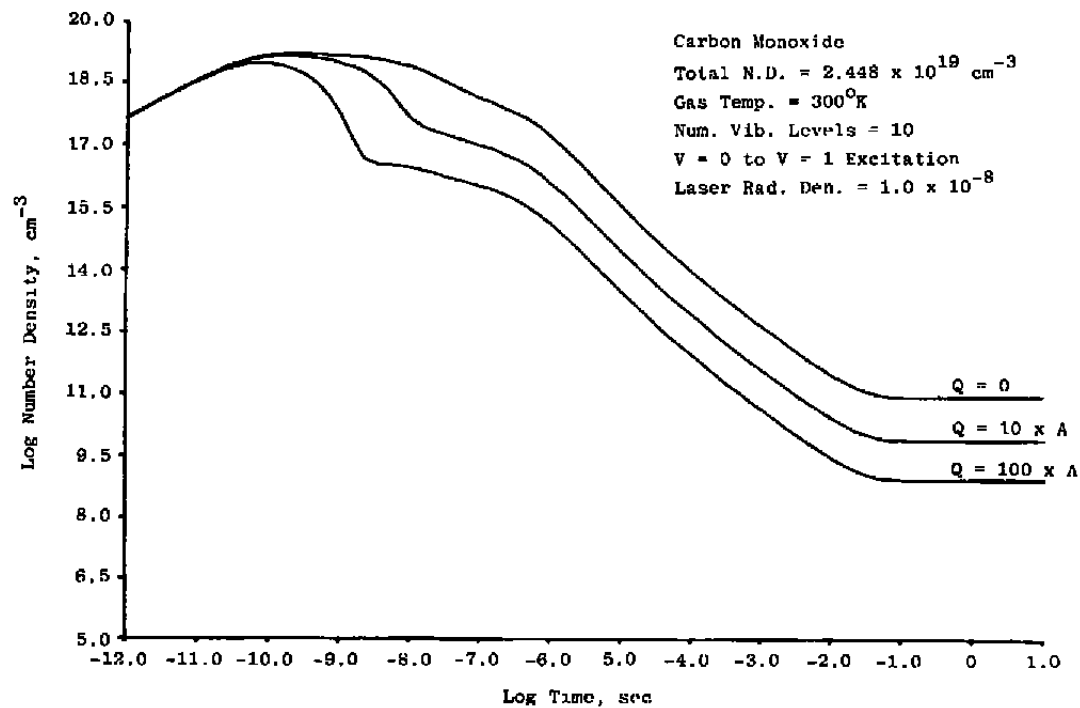
Figure 15. Time history of population in upper electronic state laser-coupled
vibrational level for three values of quenching rate.

Figure 16. Time history of vibrational population distribution in upper electronic state, T = 300°K.

Carbon Monoxide
Run Number 57
Total N.D. $= 2.448 \times 10^{19}$ cm^{-3}
Gas Temp. $= 300^{\circ}K$
Num. Vib. Levels $= 10$
$V = 0$ to $V = 1$ Excitation
Laser Rad. Den. $= 1.0 \times 10^{-8}$
$Q = 100 \times A$
Upper Elec. Level
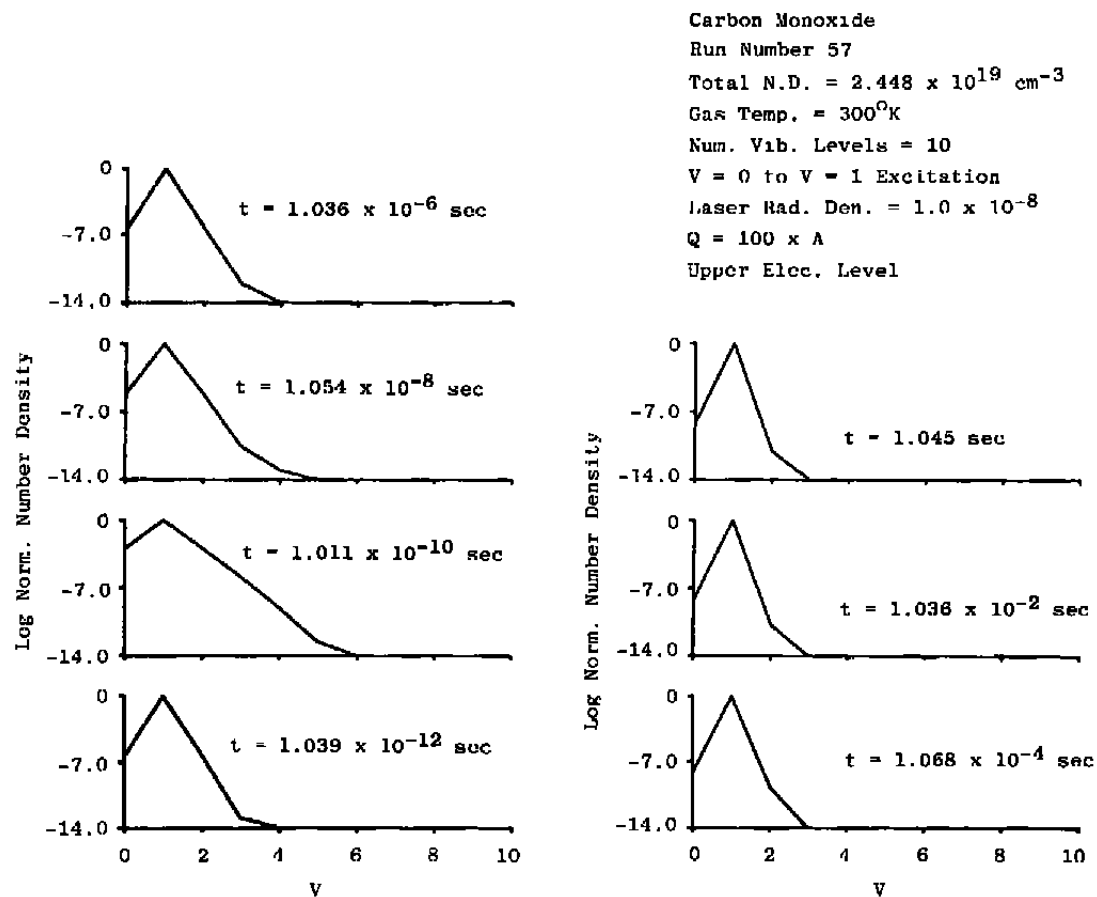
Figure 17. Time history of vibrational population distribution in
lower electronic state, T = 300°K.
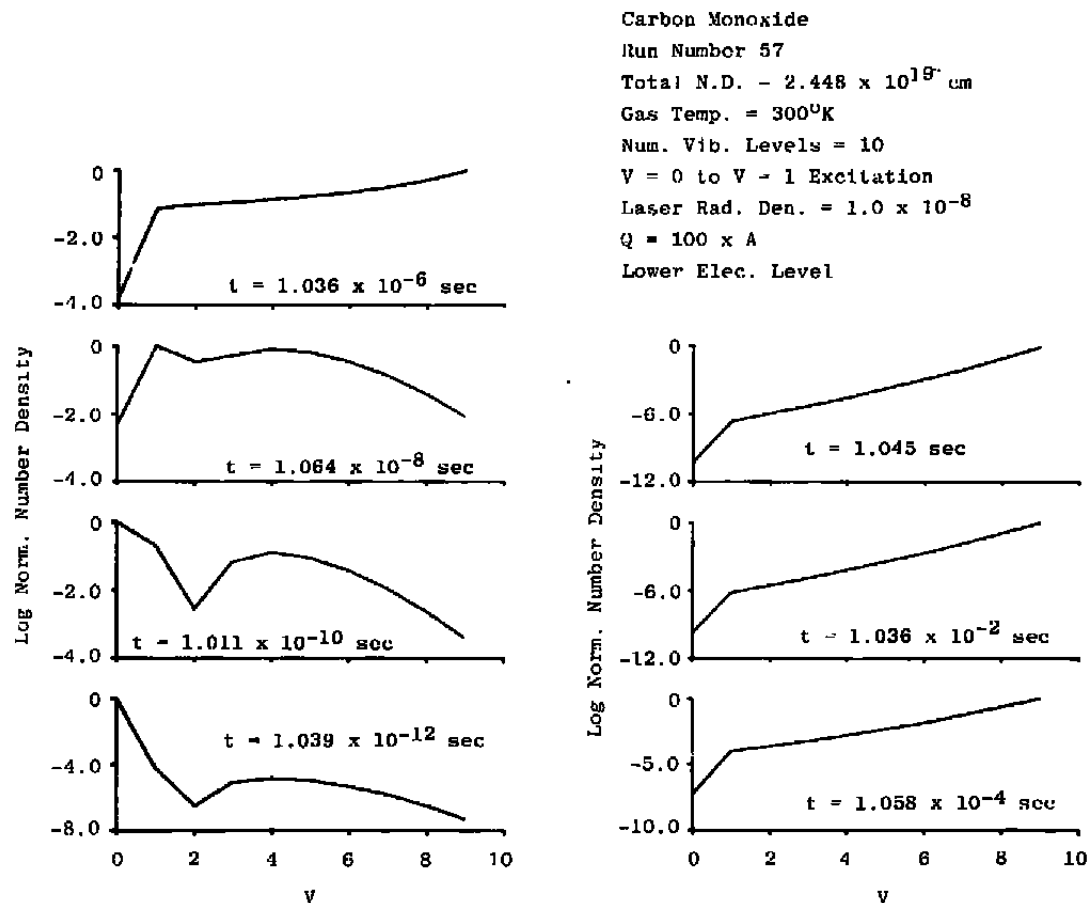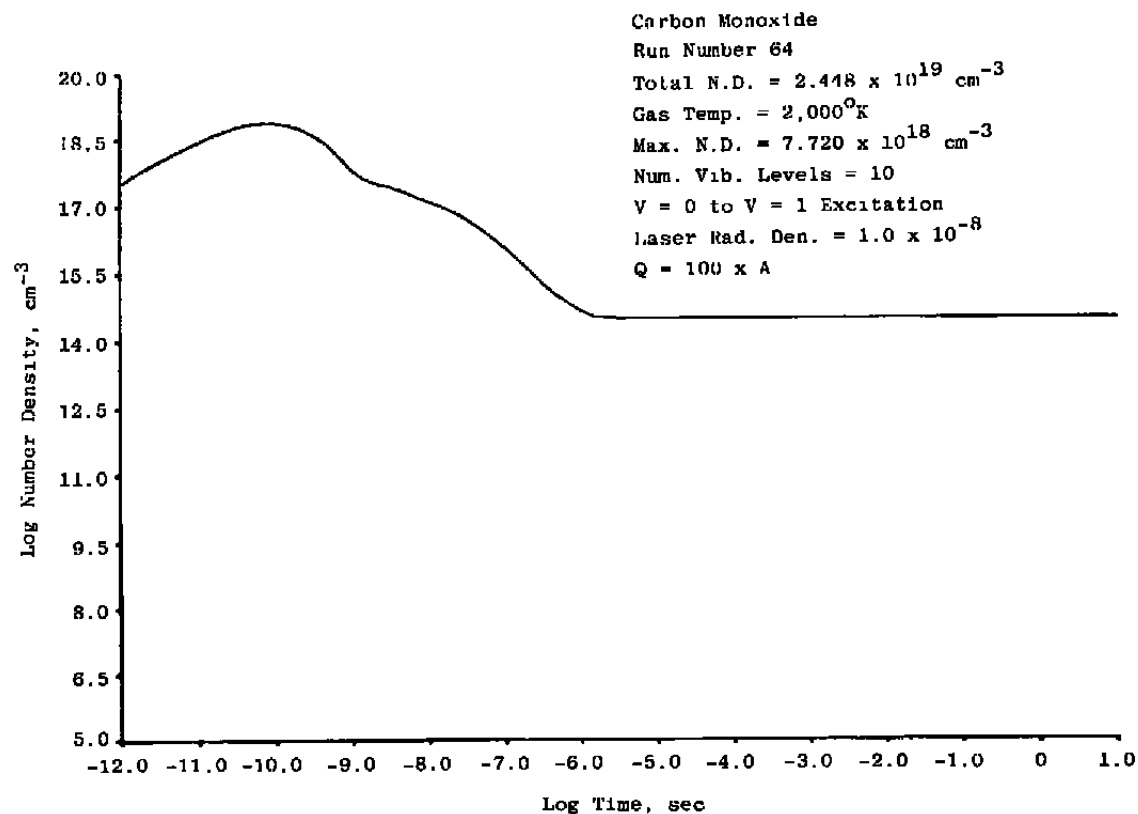
Figure 18. Time history of population in upper electronic state
laser-coupled vibrational level, T = 2,000°K.

The effects of laser radiation density on the upper vibrational level number density are presented in Fig. 19 and Table 2. In the figure is plotted the peak number density in the upper vibrational level normalized by the steady-state number density predicted by the two-level model for both 300°K and 2,000°K. At the lower temperature the peak number density is equal to the two-level model prediction for laser radiation densities greater than 10^{-6} erg cm^{-3} Hz^{-1}. The ratio falls quickly around 10^{-8} erg cm^{-3} Hz^{-1} and again levels out at a lower lower ratio for radiation densities less than 10^{-10} erg cm^{-3} Hz^{-1}. For the higher temperature case the same pattern emerges, except that at the saturated conditions the ratio is below a value of one. In Table 2 the steady-state time and number density are essentially constant for all the laser radiation densities tested at 300°K. At 2,000°K the time of steady state is virtually constant but the number density does show a reduced value at the lower radiation densities.

In summary, for saturated laser excitation of carbon monoxide the peak of the number density in the upper laser-excited vibrational level is comparable to the two-level prediction at room temperature. For lower radiation densities, for high temperatures, or for prediction of the time history and steady-state conditions, the two-level model fails completely because of the finite collisional exchange rates and large contribution of multipath radiative and collisional relaxation from the upper electronic state vibrational manifold to the ground electronic state vibrational levels.
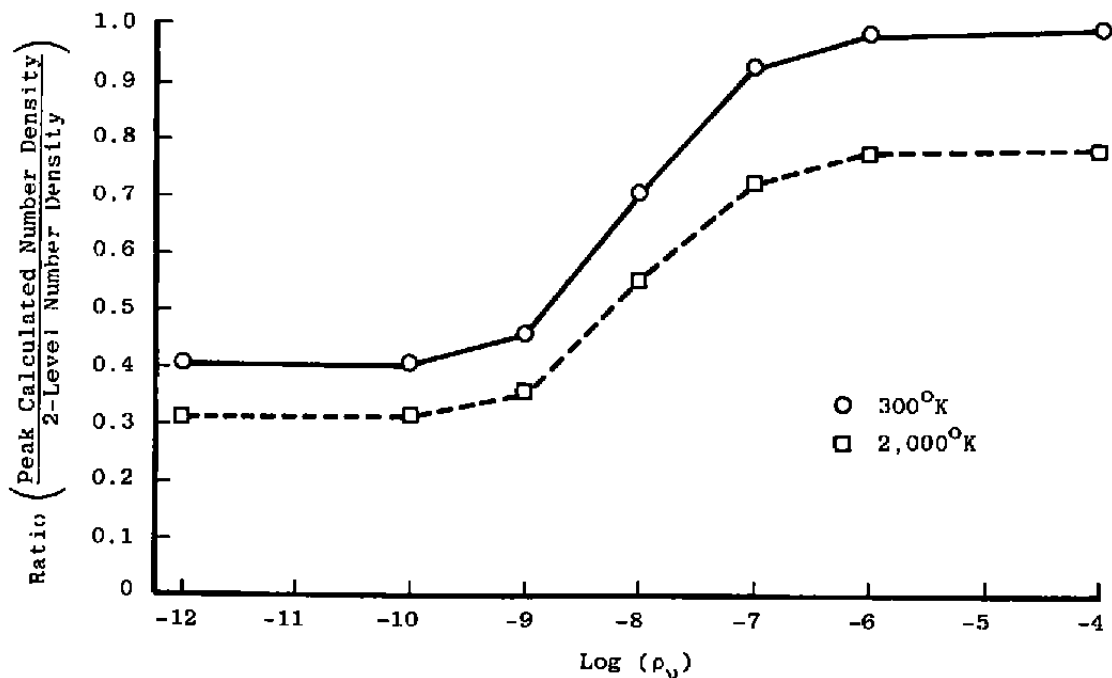
Figure 19. Laser radiation density effects on ratio of calculated peak number density and two-level model steady-state prediction.

Table 2. Maximum and Steady-State Number Densities and Times

δ_ν	Maximum	Steady State	Maximum	Steady State
10^{-4}	1.625×10^{19} 1.0×10^{-12}	8.447×10^{8} 0.2	1.275×10^{19} 1.0×10^{-12}	3.160×10^{14} 5.0×10^{-6}
10^{-6}	1.610×10^{19} 2.0×10^{-12}	8.447×10^{8} 0.2	1.264×10^{19} 2.0×10^{-12}	3.160×10^{14} 5.0×10^{-6}
10^{-8}	9.879×10^{18} 7.0×10^{-11}	8.447×10^{8} 0.2	7.720×10^{18} 7.0×10^{-12}	3.158×10^{14} 5.0×10^{-5}
10^{-10}	3.809×10^{17} 5.0×10^{-10}	8.446×10^{8} 0.2	2.987×10^{17} 5.0×10^{-10}	3.023×10^{14} 5.0×10^{-6}
10^{-12}	4.044×10^{15} 1.0×10^{-9}	8.405×10^{8} $0.2 \rightarrow 0.3$	3.172×10^{15} 1.0×10^{-9}	2.069×10^{14} 7.0×10^{-6}

Number Density (cm^{-3})
Time After Laser Radiation Initiation (seconds)

5.0 SUMMARY

The objective of this work was to assess the feasibility of using the laser-induced fluorescence technique to measure space-and time-resolved species number densities in gaseous systems. Specifically, computer codes were developed to model the detailed kinetic rate relaxation of Na atom—N_2 molecule and CO molecule systems to evaluate the usefulness of the simple two- and three-energy level models in deriving number densities from fluorescence intensities.

For sodium-nitrogen mixtures the time-dependence of the fluorescence intensity was shown to be dependent upon both the total N_2 number density and the N_2 vibrational mode number density distribution function. Specifically, it was shown that a metastable steady-state fluorescence intensity of Na was attained within 0.1 − 10 nsec after initiation of the laser source radiation. Further, the metastable steady-state fluorescence intensity for the three-level Na model was dependent upon the N_2 number density, thereby providing a means of measurement of the local N_2 number density using Na as a fluorescent tracer. As time increases, the effects of vibration-vibration and vibration-translation energy transfer processes in the N_2 assume added importance, and a transition occurs in the fluorescence signal from the metastable state to a final steady state. For the parameters used in this study it was seen that this transition occurred approximately 1 msec after initiation of the laser source radiation. Consequently, for laser pulses sufficiently long in duration to attain the metastable steady-state condition, and shorter than the time of transition to the final steady-state condition, the laser-induced fluorescence technique using the three-level model appears to be feasible for measuring nitrogen, or other similar diatomic molecule, number densities with sodium as a tracer. Experimental measurements under controlled conditions are recommended to validate further the applicability of this technique.

For molecular systems the preliminary results using pure carbon monoxide have shown the vital importance of multipath relaxation from the upper laser-excited level. For carbon monoxide the two-level model is totally inadequate for predicting the steady-state populations. Consequently, the laser-induced fluorescence technique based on the two-level model cannot be used with any degree of reliability for carbon monoxide number density measurements. Furthermore, these results make it clear that it is highly desirable to extend the computer modeling techniques developed here to more realistic multispecies molecular systems and to species of interest, such as OH, in order to evaluate the applicability of laser-induced fluorescence to these systems.

REFERENCES

1. Baronavski, A. P. and McDonald, J. R. "Application of Saturation Spectroscopy to the Measurement of C_2 $3\Pi_u$ Concentrations in Oxy-acetylene Flames." *Applied Optics*, Vol. 16, No. 7, July 1977, pp. 1897-1901.

2. Pasternack, L., Baronavski, A. P., and McDonald, J. R. "Application of Saturation Spectroscopy for Measurement of Atomic Na and MgO in Acetylene Flames." *Journal of Chemical Physics*, Vol. 69, No. 11, December 1978, pp. 4830-4837.

3. Bonczyk, P. A. and Shirley, J. A. "Measurement of CH and CN Concentrations in Flames by Laser-Induced Saturated Fluorescence." *Combustion and Flame*, Vol. 34, 1979, pp. 253-264.

4. Stepowski, D. and Cottereau, M. J. "Direct Measurement of OH Local Concentration in a Flame from the Fluorescence Induced by a Single Pulse." *Applied Optics*, Vol. 18, No. 3, February 1979, pp. 354-356.

5. Bechtel, J. H. and Teets, R. E. "Hydroxl and Its Concentration Profile in Methane-Air Flames." *Applied Optics*, Vol. 18, No. 24, December 1979, pp. 4138-4144.

6. Daily, J. W., and Chan, C. "Laser-Induced Fluorescence Measurement of Sodium in Flames." *Combustion and Flame*, Vol. 33, 1978, pp. 47-53.

7. Starr, W. L. "Excitation of Electronic Levels of Sodium by Vibrationally Excited Nitrogen." *Journal of Chemical Physics*, Vol. 43, No. 1, July 1965, pp. 73-75.

8. Lijnse, P. L. and Elsenaar, R. J. "The Temperature Dependence of the Quenching of Na-D-Doublet by N_2 and H_2O in Flames of 1500-2500 K." *Journal of Quantitative Spectroscopy and Radiative Transfer*, Vol. 12, 1972, pp. 1115-1128.

9. Krause, H. F., Fricke, J., and Fite, W. L. "Excitation of Na D-Line Radiation in Collisions of Sodium Atoms with Internally Excited H_2, D_2, and N_2." *Journal of Chemical Physics*, Vol. 56, No. 9, May 1972, pp. 4593-4605.

10. Bauer, E., Fisher, E.R., and Gilmore, F. R. "De-excitation of Electronically Excited Sodium by Nitrogen." *Journal of Chemical Physics*, Vol. 51, No. 10, November 1969, pp. 4173-4181.

11. Gear, C. W. *Numerical Initial Value Problems in Ordinary Differential Equations.* Prentice Hall, Englewood Cliffs, N. J., 1971.

12. Hertel, I. V., Hofmann, H., and Rost, K. J. "Electronic to Vibrational Energy Transfer in the Differential Scattering of Na* by N_2 Molecules." *Physical Review Letters*, Vol. 36, No. 15, April 1976, pp. 861-863.

13. Apt, J. and Pritchard, D. E. "Velocity Dependence of Fine-Structure Changing of Na with Ne, Ar, Xe, N_2 and CO_2." *Journal of Physics B: Atomic and Molecular Physics*, Vol. 12, No. 1, 1979, pp. 83-98.

14. Stupauski, M. and Krause, L. "Inelastic Collisions Between Excited Alkali Atoms and Molecules V. Sensitized Fluorescence in Mixtures of Sodium with N_2, H_2, HD, and D_2." *Canadian Journal of Physics*, Vol. 46, No. 19, October 1968, pp. 2127-2131.

15. Lucht, R. P. and Laurendeau, N. M. "Two-Level Model for Near Saturated Fluorescence in Diatomic Molecules." *Applied Optics*, Vol. 18, No. 6, March 1979, pp. 856-861.

16. Mumma, M. J., Stone, E. J., and Zipf, E. C. "Excitation of the CO Fourth Positive Band System by Electron Impact of Carbon Monoxide and Carbon Dioxide." *Journal of Chemical Physics*, Vol. 54, No. 6, March 1971, pp. 2627-2634.

17. Kibble, B. P., Copley, G., and Krause, L. "Effect of Imprisonment of Radiation in Sodium Vapor on Measured Lifetime of the 3^2P States." *Physical Review*, Vol. 153, No. 1, January 1967, pp. 9-12.

18. Pitre, J. and Krause, L. "Sensitized Fluorescence in Vapors of Alkali Metals, X. Energy Transfer in Sodium-Sodium Collisions." *Canadian Journal of Physics*, Vol. 46, 1968, pp. 125-128.

19. Kuhn, H. G. *Atomic Spectra.* Academic Press, New York, 1961.

NOMENCLATURE

A_{ij}	Einstein spontaneous emission coefficient rate for i-j transition
B_{ij}	Radiative absorption coefficient (i < j), stimulated emission coefficient (i > j)
C	Constant proportional to viewing volume and optical parameters [(Eq. (5)]
E	Energy
g_i	Statistical weight of level i
k	Boltzmann's constant
k_{ij}	Rate constant involving energy states i and j
N_i	Number density of level i
N_T	Total diatomic gas species number density
Q_{ij}	Quenching (i > j) or reverse quenching (i < j) rate
Q_T	Total quenching rate
q_{ij}	Cross section for i-j collisional exchange
$R_{i,j;v,w}$	V-V rate constant for transition from states i, j to states v, w
R_{ij}	R-T or V-T rate constant for i-j transition
S	Fluorescent signal
T	Kinetic temperature
t	Time
V-V	Vibrational-vibrational transitions

V-R	Vibrational-rotational transition
V-T	Vibrational-translational transition
v,w	Vibrational quantum level
λ	Wavelength
ϱ_ν	Excitation radiation energy density

APPENDIX A
MOLECULAR EXCHANGE RATE CONSTANTS

1.0 INTRODUCTION

The theoretical formulation of Herzfeld and Litovitz (HL) (Ref. A-1) for collisional energy exchange attributable to short range interactions is employed to calculate molecular V-V and V-T exchange rate constants. Their expressions yield values for the V-T and V-V transition probabilities (P) based on the kinetic (translational energy exchange) rate constant (R_t) at a given temperature, so that the V-T or V-V rate constant will be

$$R = PR_t \qquad (A-1)$$

the kinetic collision rate (R_t) is

$$R_t = \frac{1}{2} \sigma \bar{c}_r = d^2 \left(\frac{2\pi \, k \, T}{\tilde{m}} \right)^{\frac{1}{2}} \qquad (A-2)$$

where d is the collisional interaction radius (molecular diameter), $\bar{c}_r$ is the average relative velocity of the colliding molecules, σ the collision cross section, and $\tilde{m}$ is the reduced mass.

2.0 VIBRATIONAL EXCHANGE

2.1 V-T PROBABILITIES

Following the HL analysis, the V-T transition probability is separated into three components

$$P_{VT} \sim \frac{1}{Z_o} \frac{1}{Z_{vac}} \frac{1}{Z_{tr}} \qquad (A-3)$$

Z_o is a geometrical factor estimated by HL to be 3. Single quantum vibrational transitions only are considered in the HL formulation. For the general case of vibration exchange in molecule B-C attributable to a V-T collision with molecule A,

$$\frac{1}{Z_{vac}} = \frac{(M_B^2 + M_C^2) \, M_A}{M_B \, M_C \, (M_A + M_B + M_C)} \, \pi^2 \, \frac{\theta}{\theta'} \qquad (A-4)$$

where M_A, M_B, and M_C are the molecular weights of molecule A, atom B, and atom C respectively, θ is the characteristic temperature of the vibrational transition,

$$\theta = \frac{|F_1 - F_2|}{k} \qquad (A-5)$$

39

for vibrational energies E_1 and E_2, and finally

$$\theta' = \frac{16\pi^4 \, \widetilde{m} \, \ell^2 \, \nu^2}{k} \qquad (A-6)$$

where m is the reduced mass of the system

$$\widetilde{m} = \frac{M_A \, M_{BC}}{M_A + M_{BC}} \qquad (A-7)$$

ν is the frequency corresponding to the vibrational transition ($\nu = E_1-E_2/h$), k is Boltzmann's constant and ℓ is the range of repulsive forces between the colliding molecules. Next

$$\frac{1}{Z_{tr}'} = \frac{1}{\pi^2} \sqrt{\frac{2\pi}{3}} \left(\frac{\theta'}{\theta}\right)^2 \left(\frac{\theta'}{T}\right)^{\frac{1}{6}} \exp\left[-\frac{3}{2}\left(\frac{\theta'}{T}\right)^{\frac{1}{3}} + \frac{\theta}{2T}\right] \qquad (A-8)$$

for translational temperature T.

The final form of the HL V-T probability is

$$P_{VT} = \frac{1}{1.017}\left(\frac{r_c}{r_o}\right)^2 \frac{1}{Z_o} \frac{1}{Z_{osc}} \frac{1}{Z_{tr}'} \; Y(2,2) \, e^{-\epsilon/kT} \left(1 - e^{-\theta/T}\right)^{-1} \qquad (A-9)$$

where r_c/r_o is the ratio of the stopping point (r_c) for a molecule coming from infinity and undergoing an inelastic collision and the Lennard-Jones constant (r_o), Y(2,2) is the "Sutherland correction" factor

$$Y(2,2) = 0.76\left(1 + 1.1\,\frac{\epsilon}{kT}\right) \qquad (A-10)$$

and ϵ is the Lennard-Jones potential well depth. Table A-1 lists the values for the constants used in the sodium-nitrogen and carbon monoxide relaxation codes.

2.2 V-V PROBABILITIES

The V-V probability is similarly divided into three components:

$$P_{VV} = P_{\substack{v \to v-1 \\ w \to w+1}} = \frac{1}{Z_o} \frac{1}{Z_{osc}} \frac{1}{Z_{tr}} \qquad (A-11)$$

Table A-1. Constants for V-T, V-V and R-T Calculations

Parameter	Value	Source
σ	3.75	Ref. A-4
r_c/r_o	1.0	Approximation
ε/k	91.5	Ref. A-1
ℓ	2.117×10^{-9}	Ref. A-1
F	0.15	*
C	0.10	*

* See Appendix Section 3.0

where

$$\frac{1}{Z_{tr}} = \frac{1}{\pi^2}\sqrt{\frac{2\pi}{3}}\left(\frac{T}{\theta'_{12}}\right)^{\frac{1}{6}}\left(\frac{\theta'_{12}}{\theta_1-\theta_2}\right)\exp\left[-\frac{3}{2}\left(\frac{\theta'_{12}}{T}\right)^{\frac{1}{3}}+\frac{\epsilon}{kT}+\left(\frac{\theta_1-\theta_2}{2T}\right)\right] \quad (A-12)$$

with

$$\theta'_{12} = \frac{16\pi^4\,\tilde{m}_{12}\,k\,\ell^2\,(\theta_1-\theta_2)^2}{h^2} \quad (A-13)$$

Note that the third term in the exponential, because of the anharmonicity of vibrational motion, accounts for the difference between endothermic and exothermic collisional transfer, i.e., detailed balance effects. In the actual calculation of $1/Z_{tr}$ for both V-T and V-V probabilities, exothermic probabilities only are calculated using the full equations, with the corresponding reverse probabilities calculated using the detailed balance relation $P_{en} = P_{ex}\,e^{-\Delta E/kT}$ where ΔE is the energy given up to translation during the collision because of the mismatch in vibrational energies during the V-V exchange collision. Now,

$$\frac{1}{Z_{osc}} = 4\pi^4\left(\frac{M_B^2+M_C^2}{4M_B M_C}\right)_1\left(\frac{M_B^2-M_C^2}{4M_B M_C}\right)_2\frac{\theta_1\,\theta_2}{\theta'_1\,\theta'_2} \quad (A-14)$$

Substituting for Θ' and Θ and simplifying yields

$$\frac{1}{Z_{osc}} = \left(\frac{M_B^2+M_C^2}{4M_B M_C}\right)_1\left(\frac{M_B^2+M_C^2}{4M_B M_C}\right)_2\frac{4h^4}{16\pi^4\,\tilde{m}_{12}^2\,\ell^4\,(E_1-E_2)_1(E_1-E_2)_2} \quad (A-15)$$

41

Z_o, sometimes referred to as the steric factor, is the term which adjusts for the fact that the theoretical analysis which produces the mathematical expressions for Z_o and Z_{o}, neglects the rotational motion of the colliding molecules. HL suggest a value of $Z_o = 9$.

Figure A-1 shows the V-V and V-T transition probabilities at various translational temperatures for nitrogen. For temperatures below approximately 1,000°K the V-T probabilities for the lower vibrational levels are negligible compared to the V-V probabilities. Despite the smallness of the V-T probabilities it was necessary to include V-T transfer in the relaxation code to obtain steady-state conditions at a finite time.

For carbon monoxide it is known that long range dipole interactions play a significant role in V-V exchange processes for the lower vibrational levels (Refs. A-3 and A-4). This effect tends to increase the V-V probabilities calculated by the HL method by approximately two orders of magnitude at a temperature of 300°K for collisions involving the lower vibrational levels ($v < 10$), although the shape of the probability distribution is also altered so that the deviation from the HL probabilities is not constant for each transition. Nonetheless, for the purposes herein, which are primarily qualitative, the HL V-V probabilities multiplied by 100 are used as representative of the true V-V probabilities for carbon monoxide.

3.0 R-T RATE CONSTANTS

The exponential gap law as proposed by Polanyi and Woodall (Ref. A-2) is used to calculate the R-T probabilities. For a downward transition from J to J' the transition probability is

$$P_{JJ'} = F \exp\left[-C\left(E_J - E_{J'}\right)/kT\right] \tag{A-16}$$

where F is the normalization constant, and C is the parameter governing the exponential decrease in the probability with increasing energy gap $\Delta E = E_J - E_{J'}$.

Table A-1 gives the values of the constants in Eq. (A-16) which were used in the present analysis. These values are somewhat arbitrary because of the lack of any experimental values for the R-T exchange rates in CO. They are chosen so that the probability distribution variation with ΔJ and J approximates that found for HCl in Ref. A-2. The value of $P_{JJ'}$ for $J = J'$ ($\Delta J = 0$) is adjusted so that the total probability is equal to one.
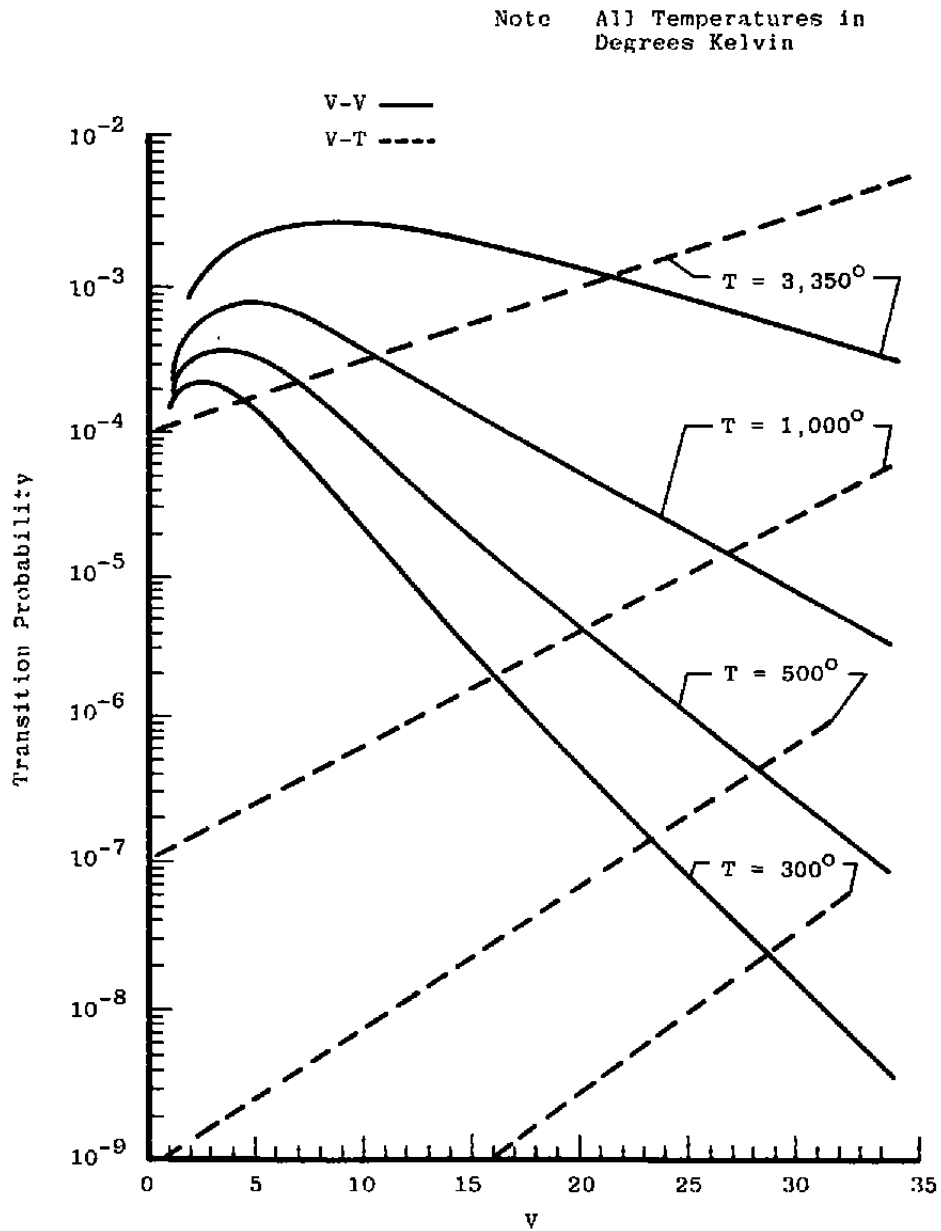
Figure A-1. Transition probability diagram.

REFERENCES

A-1. Herzfeld, K. F. and Litovitz, T. A. *Absorption and Dispersion of Ultrasonic Waves.* Academic Press, New York, 1959.

A-2. Polanyi, J. C. and Woodall, K. B. "Mechanism of Rotational Relaxation." *Journal of Chemical Physics*, Vol. 56, No. 4, February 1972, pp. 1563-1572.

A-3. Jeffers, W. Q. and Kelley, J. D. "Calculations of V-V Transfer Probabilities in CO-CO Collisions." *Journal of Chemical Physics*, Vol. 55, No. 9, November 1971, pp. 4433-4437.

A-4. Lordi, J. A., Falk, R. J., and Rich, J. W. "Analytical Studies of the Kinetics of Electrically Excited, Continuously Operating CO Flow Lasers." AIAA Paper No. 74-563, June 1974.

NOMENCLATURE

C	Exponential parameter [(Eq. (A-16)]
$\bar{c}_r$	Average relative velocity
d	Collision interaction radius (molecular diameter)
E_i	Energy of level i
F	Normalization constant [Eq. (A-16)]
h	Planck's constant
k	Boltzmann's constant
ℓ	Repulsive intermolecular force range
M_i	Molecular weight of species i
$\bar{m}$	Reduced mass
P	Transition probability

R_t Collision rate defined by Eq. (A-2)

r_c Stopping point in molecular collision

r_o Lennard-Jones constant

T Temperature

$Y(2,2)$ Sutherland correction factor

Z_o, Z_{osc}, Z_{tr} Components of vibrational transition probabilities

ϵ Lennard-Jones potential well depth

θ Characteristic temperature

θ' Term defined by Eq. (A-6)

θ_{12}' Term defined by Eq. (A-13)

ν Frequency

σ Collisional cross section